Isotopes for fundamental research

^{83m}Kr for KATRIN

and

^{101}Rh and ^{109}Cd for XRD studies on planets

Dissertation
zur
Erlangung des Doktorgrades (Dr. rer. nat.)
der
Mathematisch-Naturwissenschaftlichen Fakultät
der
Rheinischen Friedrich-Wilhelms-Universität Bonn

vorgelegt von

Makhsud Rasulbaev

aus

Frunse, Kirgisien

Bonn 2010

Angefertigt mit Genehmigung
der Mathematisch-Naturwissenschaftlichen Fakultät
der Rheinischen Friedrich-Wilhelms-Universität Bonn

1. Gutachter: Privatdozent Dr. Reiner Vianden
2. Gutachter: Professor Dr. Karl Maier

Tag der Promotion: 16.12.2010
Erscheinungsjahr: 2011

Contents

Introduction

The advantage of radioisotopic standards compared to other physical standards is the independence of their properties from outer conditions. They are neither sensitive to temperature change nor to progress of time. They serve as influence-free-etalon. That is why their use is advantageous in fundamental research, where high precision is required. For instance in direct neutrino mass measurement experiments utilizing tritium β-decay. In this process a helium ion, an electron and an electron antineutrino are emitted:

$$\mathrm{T} \rightarrow \ {}^{3}\mathrm{He}^{+} \ + \ \mathrm{e}^{-} + \ \bar{\nu}_{\mathrm{e}}.$$

Since a ^{3}He ion is massive, almost all energy is carried away by the electron and the antineutrino. Careful analysis of the electron kinetic energy at the right end of the β-spectrum (endpoint region) can bring the information about the neutrino mass.

The Karlsruhe Tritium Neutrino mass experiment (KATRIN) is a next generation tritium β-decay experiment, which aims to determine the electron antineutrino mass with one order of magnitude better than the Mainz and Troitsk experiments, namely at 0.3 - 0.35 eV/c^2. If no mass signal is observed, an upper limit for the neutrino mass of 0.2 eV/c^2 (90% C.L.) will be set. The KATRIN spectrometer is a realisation of a MAC-E-Filter (Magnetic Adiabatic Collimator combined with Electrostatic Filter) concept, to filter electrons at the endpoint interval of 18.6 keV of the tritium β-spectrum. A potential of 18.6 kV will be applied to the central electrode of the main spectrometer. The smearing out of this potential leads to imprecise knowledge about the neutrino mass. Consequently it was decided to control the potential with a high voltage divider and a nuclear standard at 3 ppm precision. The $^{83\mathrm{m}}$Kr possessing 17.8 keV conversion electron

line, which is only 0.8 keV less than the tritium β-decay endpoint is an ideal candidate for the role of a standard. The retarding voltage will be applied to the main spectrometer and a smaller spectrometer called a monitor spectrometer. On the monitor spectrometer the conversion electron line from ^{83m}Kr will be observed continuously. A potential of 800 V will be applied to a ^{83m}Kr source to give additional kinetic energy to the conversion electrons. In this work the production of ^{83m}Kr from its parent isotope ^{83}Rb and the emanation of ^{83m}Kr for the purposes of the KATRIN experiment is studied.

The second part of the current thesis concerns alternative X-ray sources for the space missions on planets, moons and asteroids of the solar system. In situ analysis of regolith and minerals at the surface of planets by means of robotized vehicles was one of the foreground research aims of space missions. X-ray diffractometry and fluorescence analysis of these materials can give insigts to better understanding of planet formation. Further, interesting data for astrobiology can be gained from the presence of water on the examined planet. There are serious constraints set on the mission's experimental equipment such as limited mass, size and power consumption. Thereby, lightweight radioisotopic X-ray emitters offer a good alternative to massive X-ray tubes. The isotopes currently used, ^{55}Fe and ^{241}Am, are not optimal for these purposes. ^{55}Fe has a low energy emission energy of 6 keV, leading to prolongation of the measurement time. The ^{241}Am having lines at 14 keV and 60 keV, suffers from a low activity per mass ratio of 126 GBq/g.

Two alternative sources for these applications, ^{101}Rh and ^{109}Cd, are investigated. Their half-lives, 3.3 years and 462.6 days respectively, are comparable with the travel time of a mission. Emission lines of the isotopes lie in 20 keV range, which contributes to effective suppression of background during the X-ray diffractometry experiments. An optimization of these isotopes' production at the Bonn Cyclotron is studied. The suitability for the X-ray diffraction experiments of ^{101}Rh is investigated.

Chapter 1

A nuclear standard for KATRIN

1.1 Motivation

1.1.1 Neutrino hypothesis and oscillations

The electron energy spectrum (β-decay) was discovered in the decay of RaB(^{214}Pb) by Chadwick in 1914 using a magnetic spectrometer. It appeared to be continuous, in contradiction to the expected monoenergetic spectrum, such as from α-emitters. The nucleus undergoing the β-transformation was in a definite state, as well as the product nucleus. Their energy difference can not be emitted continuously in a two body process. Also the resulting spin-difference between the parent and daughter nucleus was 0 or 1, but it was known that an electron carries a spin of 1/2. To rescue the energy conservation law W. Pauli postulated the existence of unknown neutral particle called Neutron[1]. In his letter to the participants of the Solvay congress he wrote (translated by K. Riesselmann):

"... Namely, the possibility that there could exist in the nuclei electrically neutral particles, that I wish to call neutrons, which have spin 1/2 and obey the exclusion principle and which further differ from light quanta in that they do not travel with the velocity of light.

The mass of the neutrons should be of the same order of magnitude as the electron mass and in any event not larger than 0.01 proton masses. The continuous beta spectrum would then become understandable by the assumption that in beta decay a neutron is emitted in addition to the electron such that the sum of the energies of the neutron and the electron is constant ..." [1].

[1] The particle known today as neutron was not discovered by then. [2]

Later the particle was renamed to neutrino (*it. small neutron*) by Fermi in his theory of β-decay [3]. According to the modern terminology an electron antineutrino is emitted in the β^- decay. The specific properties of the neutrino as a neutral charge, a very small mass, and a small magnetic moment make its registration difficult. However, in 1956 Reines and Cowan [4,5] demonstrated the existence of the neutrino. Antineutrinos were registered in an "inverse" β-decay

$$\bar{\nu}_\mathrm{e} + \mathrm{p} \rightarrow \mathrm{e}^+ + \mathrm{n}. \tag{1.1}$$

Three large liquid detectors (1.9 m $\times$ 1.3 m $\times$ 0.6 m) with photomultiplier tubes were divided through two liquid targets (7 cm width each) filled with $CdCl_2$ dissolved in water. To protect the setup from neutrons and γ-radiation, it was placed in a box made of lead and paraphine located in an underground laboratory near the Savanna River reactor. The reactor served as an antineutrino source.

An antineutrino interacting with the proton of the target solution led to the generation of a single positron and a single neutron (equation 1.1). The positron is annihilated immediately with a single electron in two monochromatic photons ($e^+e^- \rightarrow \gamma\gamma$), traced in the scintillators as a prompt signal. The neutron is slowed down in collisions with water molecules in a few microseconds and captured by a Cd nucleus following γ-emission. Thus two signals separated by a few microseconds time interval are observed on a three channel oscilloscope. In a series of long experiments, about 1400 h, it was shown that a mean of 2.88 ± 0.22 impulses are registered in an hour. It corresponds to the antineutrino-proton cross section of $\sigma = 10^{-43}$ cm^2 which is in good agreement with theory.

According to a hypothesis suggested in 1957 a muon neutrino (ν_μ) emitted in the $\pi^+ \rightarrow \mu^+ + \nu_\mu$ process is not identical to an electron neutrino (ν_e). Lederman and Schwartz [6] in 1962 showed that the hypothesis was correct: $\nu_e \neq \nu_\mu$ ($\bar{\nu}_e \neq \bar{\nu}_\mu$). In their set-up 15 GeV $\pi^\pm$ were produced through beryllium target irradiation with protons at the Brookhaven National Laboratory. In the process of $(\pi - \mu)$ decay muon neutrinos and antineutrinos were emitted. They were registered with a spark detector located at the distance of 34 m from the target. To eliminate radioactive background from the proton beam and fast $\mu^\pm$ muons the detector was shielded (up to 13.5 m steel, beton, paraphine and lead). 60

	Reaction	**Energy [MeV]**	**Name**
PP I	$p + p \rightarrow {}^2H + e^+ + \nu_e$	0.0 - 0.42	pp
	$p + e^- + p \rightarrow {}^2H + \nu_e$	1.44	pep
	${}^2H + p \rightarrow {}^3He + \gamma$	–	
	${}^3He + {}^3He \rightarrow {}^4He + 2p$	–	
PP II	${}^3He + {}^4He \rightarrow {}^7Be + \gamma$	–	
	$e^- + {}^7Be \rightarrow {}^7Li + \nu_e$	0.86, 0.38	^{7}Be
	$p + {}^7Li \rightarrow {}^4He + {}^4He$	–	
PP III	$p + {}^7Be \rightarrow {}^8B + \gamma$	–	
	${}^8B \rightarrow {}^4He + {}^4He + e^+ + \nu_e$	0 - 14.1	^{8}B
	${}^3He + p \rightarrow {}^4He + e^+ + \nu_e$	0.6 - 18.0	hep

Tab. 1.1: Neutrino producing reactions in the sun.

events were registered in a 350 h irradiation period. They were identified as a muon birth within

$$\nu_\mu + n \rightarrow \mu^- + p \; ; \; \bar{\nu}_\mu + p \rightarrow \mu^+ + n \tag{1.2}$$

reactions. An analysis showed that none of the following processes were detected:

$$\nu_\mu + n \nrightarrow e^- + p \; ; \; \bar{\nu}_\mu + p \nrightarrow e^+ + n. \tag{1.3}$$

After the detection of tau lepton (τ) in 1975 - 1978 a τ neutrino (antineutrino) was introduced. τ lepton decays through many channels always emitting a τ neutrino (ν_τ). It is believed now that the three neutrino types (flavors) ν_e, ν_μ, ν_τ are not identical.

Along with nuclear reactors the sun is a source for neutrinos. Reactions contributing to the neutrino production in the sun are listed in table 1.1 and figure 1.1. B. Pontecorvo proposed to use a tank filled with C_2Cl_4 [7] for solar

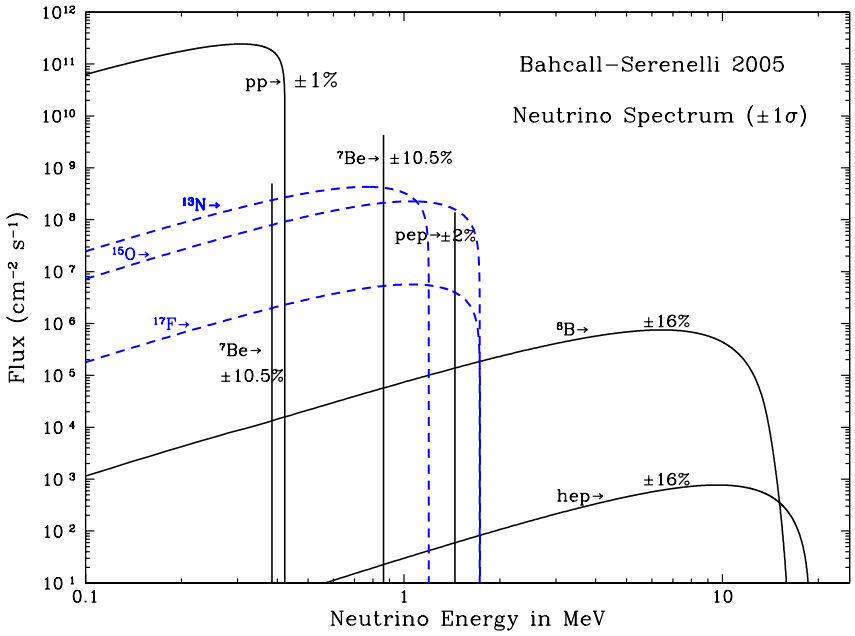

Fig. 1.1: The flux of neutrinos according to the standard solar model. Source: http://www.sns.ias.edu/∼jnb/, 15^{th} of October 2010

neutrino observation using the

$$^{37}\mathrm{Cl} \; + \; \nu_e \; \rightarrow \; ^{37}\mathrm{Ar} \; + \; e^- \tag{1.4}$$

reaction. However, he did not go further than the proposal. Later the idea was picked up by R. Davis, who carried out a series of experiments with large tanks [8] to examine the process described by equation 1.4. The ^{37}Ar was flushed in the Geiger-Müller detector with a non-radioactive ^{36}Ar carrier. The count rate obtained 2.56 Solar Neutrino Units (SNU[2]), which was about one third of the theoretical value of 7.5 SNU predicted by the standard solar model (SSM). The controversy between the experimental result and the theory raised the problem of the deficit of solar neutrinos. Many physicists believed that there was something wrong with the experiment. Davis with his colleagues tested the experiment to improve confidence in the results and never found any experimental reason for the low neutrino flux [9]. In between other theories describing the sun were proposed,

[2] 1 SNU = 10^{-36} neutrino captures per target atom per second.

however they were not able to describe all the processes occurring. J. Bahcall did not find anything wrong with the standard solar model, in fact, the advent of helioseismology confirmed the temperature profile in the model [10].

Nakagawa and Pontecorvo assumed [11, 12] that if the neutrinos have rest masses and the lepton number is not conserved, then there is a possibility of neutrino oscillations: one flavor of neutrino can (completely or partially) periodically transform into another flavor while propagating through the vacuum and matter. A characteristic dimension l of these transformations is defined by a difference of squared neutrino masses $l = 2\pi\epsilon_\nu/(m_i^2 - m_j^2)$ (here ϵ_ν is neutrino energy).

The Sudbury Neutrino Observatory (SNO) proposed by Chen [13] provided direct evidence for solar neutrino flavor change. The experiment was designed to observe non-electron neutrino flavors, allowing a flavor-independent measurement of the total neutrino flux from the sun. The experiment consisted of $1 \cdot 10^6$ kg of heavy water (D_2O) in a transparent acrylic vessel (figure 1.2). The vessel was surrounded by a stainless steel support geodesic sphere with 9456 *Hamamatsu* 20.32 cm diameter Photo Multiplier Tubes (PMT) installed "looking" inwards. $1.7 \cdot 10^6$ kg of light water was filled in the platform. Other 91 PMTs were directed outwards for the background veto unit. The vessel itself was surrounded with $5.7 \cdot 10^6$ kg of light water. The experiment was situated 2092 m below sea level (6020 m water equivalent). All PMTs were equipped with light concentrators, which increased the photo-cathode coverage to nearly 55%. In-flying particles propagating with the velocity higher than the velocity of light in water induce Cherenkov light, which is detected by PMTs. As similar water detectors the SNO was sensitive to the ^{8}B and *hep* (table 1.1) solar neutrinos. Their flavor change is observed through comparison of the flux of the neutrinos obtained from three processes:

$$\nu_x + e^- \rightarrow \nu_x + e^- \quad \text{(ES)} \tag{1.5}$$

$$\nu_e + d \rightarrow p + p + e^- \quad \text{(CC)} \tag{1.6}$$

$$\nu_x + d \rightarrow p + n + \nu_x \quad \text{(NC)} \tag{1.7}$$

The first reaction (equation 1.5), elastic scattering (ES) of electrons, has the great advantage that the recoil electron direction is strongly correlated to the direction

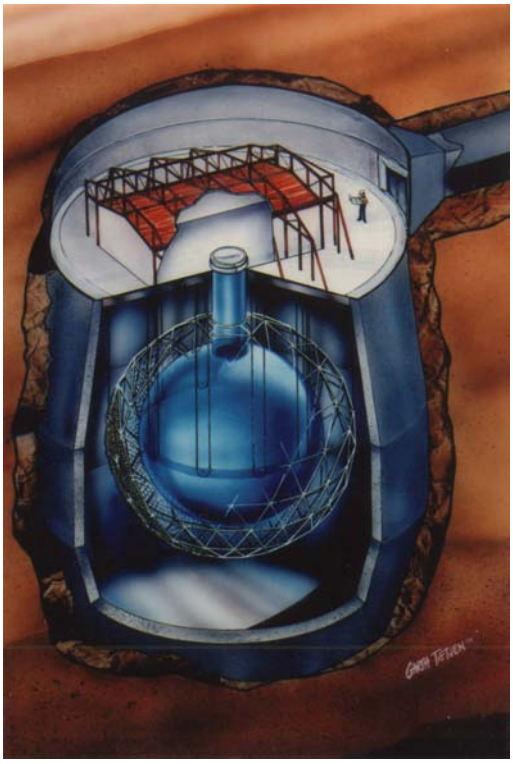

Fig. 1.2: Artist's concept of the SNO detector. [14]

of the incoming neutrino, and hence the direction to the sun. It is sensitive to all neutrino types. However, for electron neutrinos, the elastic scattering reaction has 6.5 times higher cross section compared to μ and τ neutrinos due to the presence of charged and neutral current components.

The $\nu_e - d$ charged current (CC) reaction (equation 1.6) occurs only for electron neutrinos, which interact with loosely bound neutrons in deuterium. This reaction provides exclusive sensitivity to electron neutrinos and has the advantage that the recoil electron spectrum is strongly correlated with the incident neutrino energy. It can thus provide the ^{8}B energy spectrum. The electron momentum has a weak angular correlation to the direction to the sun.

The third process (equation 1.7), also unique for heavy water, is the $\nu_x - d$ neutral current (NC) reaction, which is equally sensitive to all neutrino flavors. It thus provides a direct measurement of the total active flux of ^{8}B neutrinos from the sun. Like CC reaction, the NC reaction has a cross section nearly an order of magnitude larger than the ES reaction.

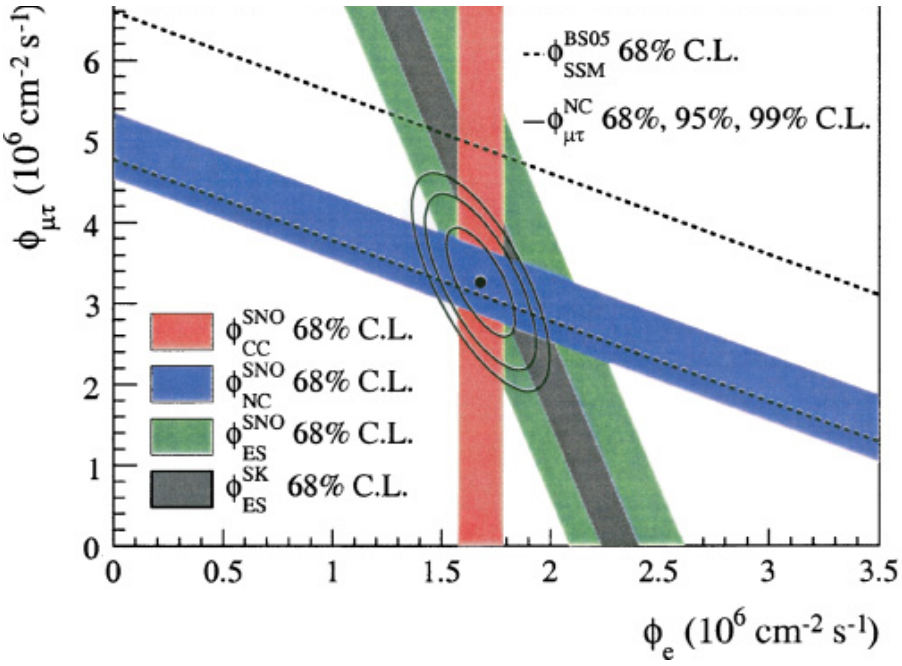

Fig. 1.3: Flux of $\mu + \tau$ neutrinos versus flux of electron neutrinos observed by SNO. CC, NC and ES flux measurements are indicated by the filled bands. The total ^{8}B neutrino flux predicted by the standard solar model is shown as dashed lines and that measured with NC channel is as the solid band parallel to the model prediction. The narrow dark band parallel to the SNO ES result correspond to the Super-KamiokaNDE result [15].

The SNO detector was designed to observe the Cherenkov light produced by ultra-relativistic electrons. The threshold for the emission of Cherenkov light is 0.767 MeV, although in practice the analysis thresholds were set much higher than this. The observed electrons produced light in a cone around the direction of the particle at a characteristic angle of approximately 42 degrees.

Electrons with sufficient energy were produced in three ways. Firstly, the ES and CC neutrino reactions produce energetic electrons directly. Secondly, gamma rays with enough energy are likely to scatter inelastically (Compton scattering) in matter, thus producing an electron which produces Cherenkov light. Most probably, however, neutron capture produces high energy gamma rays, which also have a high probability of undergoing Compton scattering, and thus produce Cherenkov light. The SNO experiment went through three different phases, each

using a different mechanism to detect the neutrinos produced in the NC reaction. The results of the experiment are shown in figure 1.3. As can be seen from comparison of the diagonal NC band with the total ^{8}B flux predicted by the standard solar model (dashed line) there is a perfect agreement of the experiment to the theory.

Neutrino oscillations is a hint on non-zero mass of neutrino. In a number of long therm experiments the mass of $\bar{\nu}_e$ was measured. For the further discussion the experiments on a direct measurement of the (anti)neutrino mass at Troitsk and Mainz are important.

1.1.2 Theory of direct neutrino mass measurements

The direct neutrino mass measurements, following Robertson and Knapp [16], are the methods that do not require for their success the non-conservation of the total lepton number or of the lepton family number. That is there is no principal difference for these experiments whether the neutrino is its own antiparticle (*Majorana neutrino*) or not (*Fermi neutrino*). These measurements are based on the concept of Fermi, who recognized already in his formulation of β-decay theory [3] that the mass of the electron neutrino could be deduced from the shape of the β-decay spectra. In the following some kinematics of the β-decay are considered to clarify this topic. The energy spectrum for a neutrino mass m_ν is given by

$$\frac{dN}{dE} = C \times F(Z,E) p (E + m_e c^2)(E_0 - E) \left((E_0 - E)^2 - m_\nu^2\right)^{\frac{1}{2}} \Theta(E_0 - E - m_\nu) \quad (1.8)$$

where E denotes the kinetic energy of the electron, m_e the mass of the electron, p is the electron momentum, E_0 corresponds to the maximum electron energy for $m_\nu = 0$ (endpoint energy). $F(Z,E)$ is the Fermi function, taking into account the Coulomb interaction of the outgoing electron in the final state. The step function $\Theta(E_0 - E - m_\nu)$ ensures energy conservation, and C is given by

$$C = \frac{G_F^2}{2\pi^3} \cos^2\theta_C |M|^2 \quad (1.9)$$

where G_F, θ_C, M are respectively the Fermi constant, the Cabibbo angle and the nuclear matrix element. As both M and $F(Z,E)$ are independent of m_ν, the

independence of the special shape on m_ν is given by the phase space factor only.

The signature of an electron neutrino with a mass of $m_\nu = 1$ eV is shown in figure 1.4 in comparison with the undistorted β-spectrum of a massless ν_e. The spectral distortion is statistically significant only in a region close to the maximum electron kinetic energy (endpoint energy) since there the neutrino has a minimum kinetic energy. Therefore only a very narrow region close to the endpoint E_0 is analyzed. As the fraction of β-decays in this region is proportional to a factor ${E_0}^{-3}$, a very low endpoint energy of the β-decay is demanded from the isotope used in the experiments. Because of the number of factors listed below, tritium has been the isotope of choice for these experiments: Tritium transforms into $^3\mathrm{He}^+$ ion emitting a single electron and an electron antineutrino within a moderate half-life of 12.3 years,

$$^3\mathrm{H} \quad \rightarrow \quad ^3\mathrm{He}^+ + e^- + \bar{\nu}_e. \tag{1.10}$$

It has the second lowest endpoint energy of 18.6 keV which maximizes the fraction of β-decays in the mentioned region. ^{187}Re has in fact seven times lower endpoint energy than tritium, but a long half-life, $5 \cdot 10^{10}$ years, puts a demand on a considerably higher amount (approximately 12,000 kg of ^{187}Re) for a similar experiment.

Further advantages of tritium as β-emitter in ν_e mass investigations are that tritium and its daughter isotope, the $^3\mathrm{He}^+$ ion, have a simple electron shell configuration. Thus, atomic corrections for the β-decaying atom- or molecule-corrections due to the interaction of the outgoing β-electron with the tritium source can be calculated in a simple and straightforward manner. For the same reason (low nuclear charge Z) the inelastic scattering of out-going β-electrons within the β-source is small. The tritium β-decay is a super allowed nuclear transition. Therefore, no corrections from the nuclear transition matrix elements M have to be taken into account.

Nevertheless, the challenges on tritium β-decay experiments are high. An example, the fraction of β-decays falling into the last 1 eV below the endpoint E_0 is only 2×10^{-13} (see the shaded region in figure 1.4), hence tritium β-decay experiments with high neutrino mass sensitivity require a huge luminosity combined

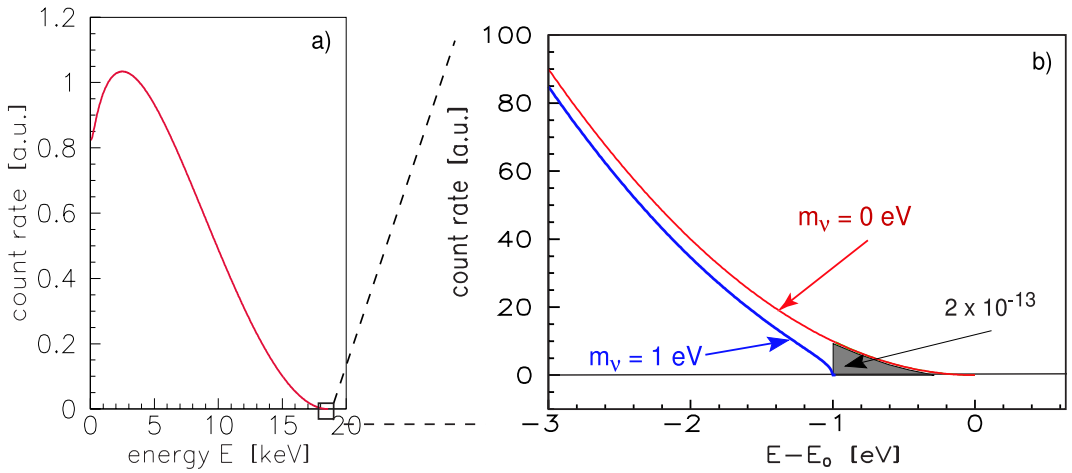

Fig. 1.4: The electron energy spectrum of tritium β-decay: (a) complete and (b) narrow region around endpoint energy E_0. In (b) the β-spectrum is shown for two neutrino mass scenarios, $m_\nu = 0$ eV and $m_\nu = 1$ eV.

with a very high energy resolution.

1.1.3 Troitsk and Mainz experiments, MAC-E-Filter

Experiments at Troitsk and Mainz pointed on the up to now lowest upper limit of the neutrino mass of 4.4 eV with 95% C.L. This was achieved with a new type of spectrometer, the so called MAC-E-Filter (Magnetic Adiabatic Collimation combined with Electrostatic Filter). It is a key element of the planned KATRIN experiment as well (see section 1.2). This concept was invented for the search for the electron neutrino mass at Troitsk and Mainz [22, 23]. The MAC-E-Filter combines high luminosity and low background with a high energy resolution, both essential to measure the neutrino mass from the endpoint region of a β-decay spectrum. Its main components are shown in the figure 1.5 illustrating the function principle as it was realized at Mainz. The Troitsk tritium source setup is more complex. Two superconducting solenoids at the left hand side and right hand side of the drawing produce a magnetic guiding field for the β-electrons from the tritium source. They start from the source into the forward hemisphere, are guided magnetically on a cyclotron motion around the magnetic field lines into the spectrometer, thus resulting in an accepted solid angle of up to 2π. On their way the magnetic field B drops by many orders of magnitude reaching its minimal

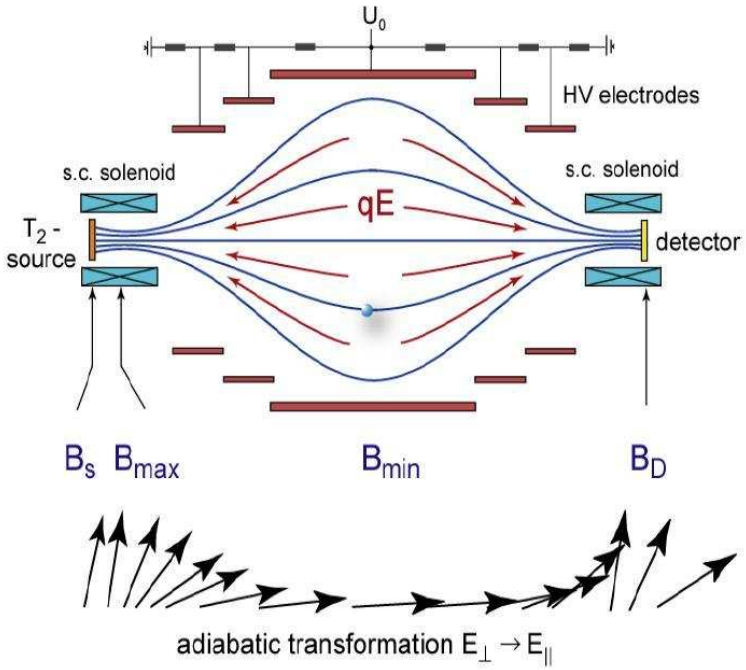

Fig. 1.5: Schematic presentation of the MAC-E-Filter (upper part of the drawing) and the transformation of the momentum vector of β-electrons [46].

value B_{min} at a medial plane of the spectrometer, further called analysing plane. Therefore, the magnetic gradient force transforms most of the cyclotron energy $E_\perp$ into longitudinal motion. This is illustrated by a momentum vector in the lower part of figure 1.5. The analyzing plane is almost parallel to the magnetic field lines which play a role of a collimator. Due to the slowly varying magnetic field the momentum transforms adiabatically, therefore the magnetic moment μ keeps constant (equation given in non-relativistic approximation):

$$\mu = \frac{E_\perp}{B} = const. \tag{1.11}$$

The parallel beam of electrons runs against an electrostatic potential U, formed by a system of cylindrical electrodes. All electrons with enough energy to pass the electrostatic barrier eU are re-accelerated and collimated onto a detector, all others are reflected. It can thus be imagined that the spectrometer acts as an integrating high-energy pass filter. The relative sharpness $\Delta E/E$ of this filter is given by the ratio of the B_{min} to the magnetic field B_s between β-electron source

and spectrometer:

$$\frac{\Delta E}{E} = \frac{B_{min}}{B_s} \ . \tag{1.12}$$

Varying the electrostatic retarding potential allows measuring the β-spectrum in an integrating mode. A magnetic field B_s is applied to the electron source in order to suppress electrons which have a very long path within the tritium source and therefore possess a high scattering probability (see figure 1.5), which is lower than the maximum magnetic field B_{max}. This restricts the maximum accepted starting angle of the electrons θ_{max} by the magnetic mirror effect to:

$$\sin\theta_{max} = \sqrt{\frac{B_s}{B_{max}}} \tag{1.13}$$

Following the equations 1.11, 1.12 and 1.13 the normalized transmission function of the MAC-E-Filter with retarding potential U is analytically given for an isotopic electron source of energy E by

$$T(E,qU) = \begin{cases} 0 & : \quad E - qU < 0 \\ \dfrac{1 - \sqrt{1 - \dfrac{E-qU}{E}\dfrac{B_s}{B_A}}}{1 - \sqrt{1 - \dfrac{\Delta E}{E}\dfrac{B_s}{B_A}}} & : \quad 0 \leq E - qU \leq \Delta E \\ 1 & : \quad E - qU > \Delta E \end{cases} \tag{1.14}$$

where q denotes the electron charge. Summarizing, the spectrometer transmission function for a strictly monochromatic line with a change in the stopping potential will present a step function whose edge is smeared by the value ΔE which determines the spectrometer energy resolution.

The application of Mainz data showed that the most of the cyclotron energy is transformed into longitudinal motion except for a small rest. It lies between zero (for the emission at $\theta = 0$) and a maximum value for the emission at $\theta \approx 90°$

$$\Delta E = \frac{8 \cdot 10^{-4}\ \mathrm{T}}{2.4\ \mathrm{T}} \cdot 18\ \mathrm{keV} \approx 6\ \mathrm{eV}. \tag{1.15}$$

The source of Mainz experiment consisted of 40 monolayers of molecular tri-

Experiment	$m_\nu^2 c^4$ [eV^2]	$E_{00} = Q$ [eV]	$m_\nu c^2$ [eV]	**Ref**
(a) Tokyo	$-65 \pm 85 \pm 65$	18572.1 ± 3.0	< 13	[25]
(b) Los Alamos	$-147 \pm 68 \pm 41$	18570.5 ± 2.0	< 9.3	[26]
(c) Zürich	$-24 \pm 48 \pm 61$	18573.3 ± 0.2	< 11.7	[27]
(d) Livermore	$-130 \pm 20 \pm 15$	18568.5 ± 2.0	< 7.0	[28]
(e) Mainz	$-0.6 \pm 2.2 \pm 2.1$	18574.8 ± 0.6	< 2.3	[29]
(f) Troitsk	$-2.3 \pm 2.5 \pm 2.0$		< 2.05	[30]

Tab. 1.2: Tritium neutrino experiments.

tium (T_2) frozen at 2.8 K at an aluminum substrate. A 25 mm diameter silicon counter segmented into 5 equal areas served as a detector. The results of the Troitsk and Mainz experiments along with other experiments are shown in table 1.2. Surprisingly, all values for m_ν^2, without any exception, are negative. Experimentally negative m_ν^2 is seen in a "oveshoot" of events at the endpoint as compared to the theoretical formula of β-spectrum. The problem of negative m_ν^2 value is not well understood; there is a number of explanations:

- A systematic error of unknown reason in one, or even all experiments.
- A systematic error in the theory.
- An anomaly of the endpoint energy region.
- An imprecision in the theoretical formula of β-spectrum.

Thus, there is no convincing explanation of the negative m_ν^2 values until now – further theoretical and experimental investigations are necessary.

1.2 The KATRIN experiment

KArlsruhe TRItium Neutrino mass experiment (KATRIN) is a next-generation direct neutrino mass search experiment [21], which utilizes the tritium β-decay. The experiment will improve the neutrino-mass sensitivity compared to Mainz and Troitsk [22, 23] experiments by one order of magnitude.

The new reference design [24] has a discovery potential of 5 σ (3 σ) for a neutrino mass m_ν= 0.35 eV/c^2 (m_ν= 0.3 eV/c^2). If no neutrino mass signal is observed, an upper limit of 0.2 eV (90 % C.L.) will be set. The KATRIN will allow the investigation of the sub-eV neutrino mass scale, which is of particular interest for particle physics, astrophysics and cosmology. In contrast to other methods such as the search for neutrinoless double β-decay ($0\nu\beta\beta$) or cosmological ν-mass studies using large scale structure (LSS) and cosmic microwave background radiation (CMBR) data, the KATRIN will complement the other laboratory and cosmological methods to investigate neutrino masses. The combination and comparison of the results from tritium β-decay, neutrinoless double β-decay and cosmological studies will be essential for the understanding of the role of neutrinos in our physical world, both at the micro- and macro- scale.

1.2.1 Tritium sources and other tritium related parts of the KATRIN experiment

The Windowless Gaseous Tritium Source

The Windowless Gaseous Tritium Source (WGTS) will be a standard electron source for KATRIN. It offers high luminosity and small systematic uncertainties. Tritium of 95% purity will be fed through a number of capillaries in the middle of the 10 m long WGTS tube with a diameter of 90 mm. After injection the T_2 molecules are transported over a length of 5 m to both tube ends by diffusion. A reference column density of $\rho d = 5 \cdot 10^{17}$ molecules/cm^2 is a main source for uncertainty, that is why it should be controlled with a precision of $\pm 0.1\%$. For that a knowledge is required over number of parameters such as the tube temperature and the tritium feed rate. A technical solution is to keep the temperature of the tube at 27 K $\pm$ 30 mK by means of a two-phase neon cooling, and to achieve a tritium injection rate of 4.7 Ci/s $= 1.7 \cdot 10^{11}$ Bq $\approx$ 40 g T/day with a stability of $\pm 0.1\%$. Solenoids along the WGTS will provide a field of $B_s = 3.6$ T to guide the flow of β-electrons. A solenoid at the end of the WGTS tube will be set to 5.6 T so that the angle of accepted out-flying electrons in the WGTS is $\theta_{max} = 51^\circ$ and the accepted source area is $A_s = 53$ cm^2. It results in a guided magnetic flux of 191 T $\times$ cm^2. To keep an electrical potential over the volume constant the

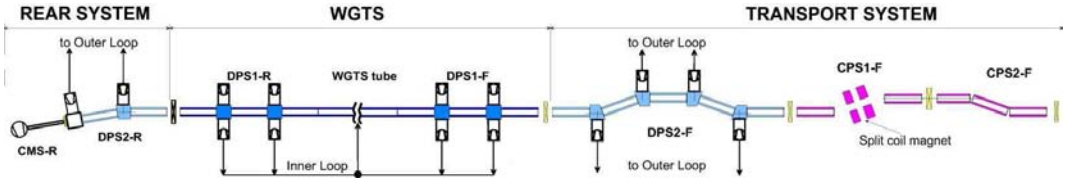

Fig. 1.6: Tritium related parts of the KATRIN experiment.

inner surface of the tube will be gold plated. Thus the WGTS using a maximum specific activity i. e. high signal rate provides a perfect homogeneity over the source cross section.

Transport and rear systems

The background generated by tritium decay within the main spectrometer must be less than 10^{-3} counts/s, which limits the amount of tritium permissible in the main spectrometer equivalent to a partial pressure of tritium of about 10^{-20} mbar. This leads to a maximal allowed tritium flow rate into the pre-spectrometer of the order of 10^{-14} mbar l/s. The tritium inlet rate is about 2 mbar l/s. This design criterion requires that the tritium flow is suppressed by about a factor of 10^{11} between the outlet of the WGTS tube and the entrance of the pre-spectrometer. This very large suppression factor is achieved by an effective tritium pumping system, based on a combination of differential (DPS) and cryogenic (CPS) pumping sections.

The first part of the tritium flow suppression is based on differential pumping. A series of pumping ports, instrumented with turbo-molecular pumps (TMP's) with high pumping capacity, reduces the tritium flow, both at the rear and front.

The differential pumping system will reduce the tritium flow to such a low level that the subsequent passive cryo-trapping system CPS will receive a tritium load of less than 1 Ci over a period of 60 days, which is equivalent to a standard tritium run cycle. The beam tube of the CPS is kept at a temperature of 4.5 K. At this temperature tritium molecules are passively adsorbed onto the liquid helium cold inner tube surfaces. To enhance the trapping probability for tritium molecules, the cold surfaces of the CPS transport tubes are anticipated to be covered by a thin layer of argon frost.

The tritium related components of the KATRIN experiment are depicted in

figure 1.6.

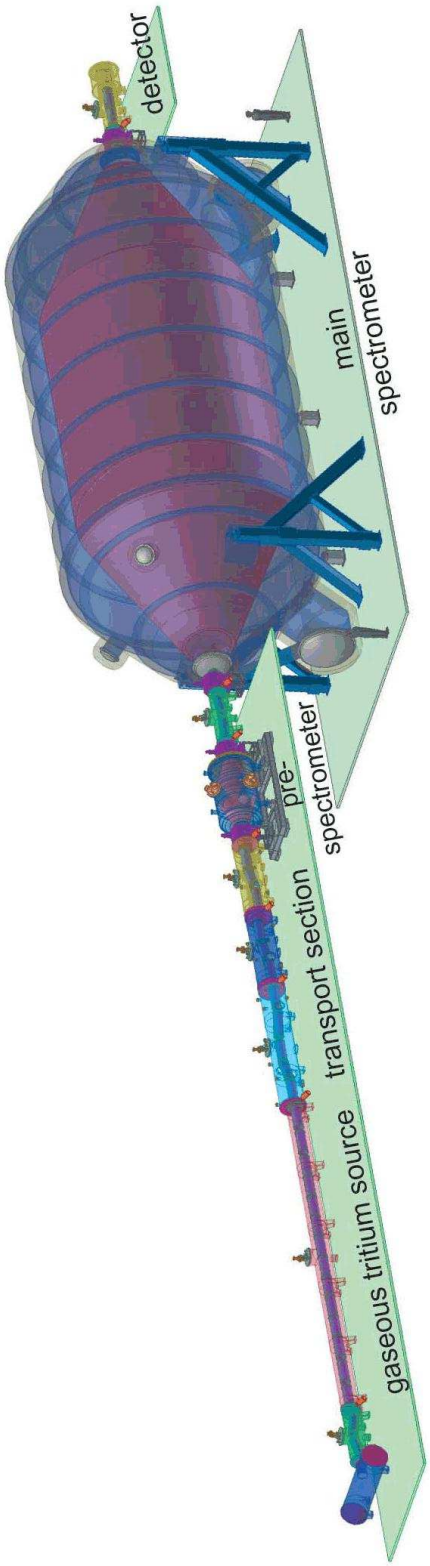

Fig. 1.7: Components of the KATRIN experiment: the windowless gaseous tritium source (WGTS), the transport section, the pre-spectrometer, the main spectrometer and the detector.

1.2.2 Electrostatic spectrometers

The electrostatic system

The electrostatic system of the KATRIN (cf. figure 1.7) consists of a pre- and a main spectrometers of the MAC-E-Filter type in a tandem setup[3]. The pre-spectrometer will filter out the electrons with energies lower than 18.3 keV. These are the electrons carrying no information about the electron neutrino mass. It will reduce the electron flux from 10^{10} s^{-1} to 10^{4} s^{-1}, which can otherwise contribute to a higher background through ionization of gas molecules in the main spectrometer. The pre-spectrometer has rather moderate energy resolution of 100 eV with a pressure requirement of e<u>X</u>treme <u>H</u>igh <u>V</u>acuum (XHV) of 10^{-11} mbar. To have a relative simple geometry of the vessel surface to reach a good vacuum it was decided to put a high voltage directly to the hull of the pre-spectrometer. A simple and lightweight inner electrode double layer system will be kept at a slightly lower potential to suppress the background from the cosmic muons and provide electrical screening. Additionally its design serves shaping of the electric field to avoid Penning traps.

Electrons which pass the pre-spectrometer symmetry plane fly into the main spectrometer. The latter with an inner diameter of 9.8 m, 23.28 m length, will be set at 18.6 keV potential at central electrode, scanning the endpoint energy of the tritium β decay with the resolution of 0.93 eV. This is a factor of 5 better than previous MAC-E-Filters at Troitsk and Mainz experiments. Residues of water and impurities on the inner surface of the vessel will be removed before the beginning of the main phase of the experiment evacuating it into XHV added baking up to 350°C with oil tube heating. A magnetic flux may reach a diameter of 9 m. As in the case of the pre-spectrometer an effort to background suppression will be attempted. 200 double layer wire modules (20-30 kg each) will be installed inside the main spectrometer volume. A high voltage supply system will provide the necessary voltage to the modules. Again as in the case of the pre-spectrometer the electrons passing the analytic plane will be re-accelerated to their initial energies and magnetically guided by the 2 - solenoid detector transport system to the final

[3] A third spectrometer of a MAC-E-Filter type, called a monitor spectrometer, is described in section 1.3.1

plane detector.

The Final Plane Detector

The detector is a multi pin diode array with an area of 63 cm^2 and a sensitivity to electrons in the range from 5 to 50 keV. It is placed downstream of the main spectrometer in a magnetic field of $B_{det} = 3$T the detector solenoid thread of 9 cm diameter. A maximum angle of incoming electrons $\theta_{det,\ max} = \arcsin(\sqrt{\frac{B_{det}}{B_{max}}}) = 45°$ is covered. With the resolution of 600 eV there is a factor of 2 improvement in the performance compared to the silicon detectors used at Mainz and Troitsk, which had 1.4 keV resolution [31, 32].

Apart from detecting electrons from tritium β-decay with energies up to 18.6 keV, the detector will be applied for the detection conversion electrons from ^{83m}Kr with energies from 17.8 keV up to 32 keV and electrons from a high rate electron gun.

1.3 Experimental

1.3.1 Calibration sources and their production

An inaccuracy σ in knowledge of the retarding potential energy E_{ret} in direct neutrino mass experiments, such as KATRIN, leads to an incorrect value of the electron neutrino mass. Its estimate was proposed by Robertson and Knapp [16]

$$\Delta m_\nu^2 = -2\sigma^2. \tag{1.16}$$

Thereby requiring the uncertainty of m_ν^2 caused by this smearing σ, to be less than 0.005 eV^2. The retarding potential energy E_{ret} depends on the scanning potential difference U_s. The last is in the range of hundreds of volts, that is why its precise measurement causes no serious problem. In case of E_{ret}, accuracy has to be in the range of 3 ppm. It was shown [40] that an unrecognized shift of E_{ret} by 0.05 eV would result in the systematic error of the fitted neutrino mass as large as 0.04 eV, which is a substantial part of the expected KATRIN sensitivity to m_ν. Several independent methods to monitor the retarding potential will be

utilized in the KATRIN experiment to achieve a high degree of redundancy.

Direct retarding potential measurement

The retarding voltage U, graded down to about 10 V by high-precision voltage divider, will be measured with a precise digital voltmeter. This project is developed and discussed by T. Thümmler for the KATRIN collaboration [36].

Monitor spectrometer

Calibration and control cannot be carried out in the main system during the tritium run. However, in accordance with equation 1.16 monitoring of the stability of the retarding voltage should be performed on a continuous basis. Thence, it was decided to apply the retarding voltage to the monitor spectrometer (old Mainz MAC-E-Filter), employing it to monitor a well defined, sharp photo- or conversion electron line from the decay of suitable radioactive isotope. The position of this line on the energy scale would be compared to the retarding energy of the main spectrometer.

Direct calibration of the main spectrometer

Additionally in between the runs the radioactive source of the type described below will be positioned in the frontal opening of the main spectrometer for an absolute calibration of the retarding energy E_{ret}. All three methods will be used not only to monitor the stability of the KATRIN retarding energy, but also to perform an absolute energy calibration repeatedly. The absolute calibration is necessary to check the stability of all monitor systems, and to compare the endpoint energy E_0, obtained by fitting the measured tritium β-spectrum with the helium-tritium mass difference $\Delta m(^3\mathrm{He} - ^3\mathrm{H})$, determined by cyclotron resonance measurements in Penning traps. Any significant difference would point to an unrecognized systematic error.
To keep the statistical error small, candidate nuclear isotopes should have a transition with a narrow line width, good reproduction of the line position, and high count rate. Sources also should be easy-to-handle. The sources with a short half-life have to allow for express deposition of a radioactive film in order to decrease

the measurement time. Mainly it should be possible to place a sufficiently strong source in the monitor spectrometer without disrupting the main measurement and at the same time a shift of the electron line neither by self absorption nor by any residual gas adsorbed on the surface of the source should occur. Under circumstances is a positioning directly in front of the main spectrometer for the determination of the transmission function necessary. The isotopes considered as candidates are discussed below.

The isotope ^{109}Cd

An application of the ^{109}Cd isotope with the half-live of $T_{1/2} = 462.6$ dhas not been investigated yet. However the source is under consideration. During the decay of ^{109}Cd into ^{109}Ag by electron capture, Auger electrons with an energy of 18.5 keV are emitted. Compared with other sources, the larger line width of 11.2 eV, leads to a demand of a higher count rate. It is also not known, whether the source undergoes a chemical change with the progress of time. Another interesting application of the ^{109}Cd radioisotope is considered in the section 2.3 of this thesis.

The Am/Co source

An operating principle of the combined Am/Co source is based on the photoelectric effect. A thin cobalt foil is placed in front of a solid ^{241}Am source. Having a line width of $\Gamma = 1.2$ eV the photoelectrons are ejected by α-particles from the K shell of cobalt with the kinetic energy of $E_{photo} = 18,635$ eV:

$$E_{photo} = E_\gamma - E_B - E_{rec} \tag{1.17}$$

Hereby, E_{photo} is the energy of photoelectrons, $E_\gamma = 26344.6 \pm 0.2$ eV the energy of emitted photons from americium, $E_B = 7708.78 \pm 0.02$ eV the binding energy of electrons in the K shell of cobalt and $E_{rec} < 0.2$ keV the recoil energy of an atom after emitting photoelectrons. An advantage of this source is a long half-life of 432 years that allows exploitation of only one source for the whole period of measurements. However, there is also a disadvantage: cobalt must have only one thin layer for electrons not to lose their energy by passing through the solid. The

group from Prague tested this source in the Mainz Spectrometer [37]. 2 counts per second within background of 9 counts per second were observed. This may lead to a measurement time of a few hours. Only then enough statistics can be achieved to test whether there is a change in voltage. Until now, the long term stability of the source is not clear.

Condensed ^{83m}Kr source and solid ^{83}Rb source

^{83m}Kr emits mono-energetic conversion electrons from the 32.1 keV and the 9.4 keV transitions of the isomeric 41.5 keV state [22]. For KATRIN monitor measurements electrons emitted from the 32.1 keV internal transition (further in text called K32 line) is the most interesting one, since their kinetic energy, $E_{K32} = 17.82$ keV, is close to the tritium endpoint, 18.6 keV. The conversion factor is high, $\alpha = 2065$.

In the case of the condensed krypton source (CKrS), ^{83m}Kr gas will be condensed on the highly oriented pyrolitic graphite substrate (HOPG) on a copper cold finger at 20 K. Cleaning of the backing with a laser beam and application of pure ^{83}Kr gas should guarantee the stability of kinetic energy of the conversion electrons. The CKrS will be used together as a part of the monitor spectrometer for the high voltage monitoring and calibration.

A short half-life of 1.83 h of ^{83m}Kr excludes the risk of spectrometer contamination, however a repeated gas condensation is required. For the experiments a considerable activity of ^{83m}Kr is necessary, but again due to its short half-life, it is unfeasible to produce this isotope in direct accelerator reaction. Luckily, the ^{83m}Kr isomeric state is fed by the parent isotope ^{83}Rb ($T_{(Rb)1/2} = 86.4$ d) with a branching ratio of 74.7%.

Another option on the continuous K32 source would be a thin evaporated layer of ^{83}Rb or usage of ^{83}Rb implanted into a platinum foil. Using a solid ^{83}Rb source, it is necessary to guarantee, that the ^{83}Rb compounds will not escape from the foil and contaminate the spectrometer. In this work the ^{83m}Kr/^{83}Rb production for the KATRIN experiment with further adsorption studies of ^{83m}Kr is discussed.

Fig. 1.8: The region of the chart of nuclides with Z = 35, Z = 37. [35]

Production of ^{83}Rb/^{83m}Kr generator

Two efficient reactions are applied by the KATRIN collaboration for the ^{83}Rb production: The ^{nat}Kr(p, xn)^{83}Rb reaction has a maximum reaction cross-section of $\sigma = 500$ mb, and a very high yield 85 MBq/10 h. Its suitability for the KATRIN experiment was investigated by Venos et al. [33]. Rubidium is gained at the U − 120M cyclotron at Řež with an average current of 6 μA, and an initial proton energy of 27 MeV. The main challenges here are the necessity to use a high pressure Kr gas target (7 bars, 22 cm^3) and the technique to remove and store the ^{83}Rb produced from the gas stream.

The second route is the production in ^{nat}Br(α, 2n)^{83}Rb reaction at the Bonn Isochronous Cyclotron. Its feasibility of is discussed in [39]. In the present chapter the technical details of the ^{83}Rb production from ^{nat}Br(α, 2n)^{83}Rb reaction are described.

Natural bromine possess two stable isotopes (^{79}Br and ^{81}Br) with almost equal abundance 50.69 %, and 49.31 %, respectively (figure 1.8). In order to achieve a production rate as large as possible a liquid target of natural bromine, ^{nat}Br$_2$, was chosen. This ensures the highest ^{81}Br density (3.119 g/cm^3 at R.T.), and should allow an effective removal of the beam energy deposited in the target. Since liquid bromine has high chemical reactivity the only suitable containers are

tubes made of quartz.

The rubidium production rate can be estimated from the incident α-beam intensity Φ, the cross section σ, the density of target atoms n and the target thickness d:

$$\frac{dN(Rb)}{dt} = \Phi \cdot \sigma \cdot n \cdot d \tag{1.18}$$

the density n can be expressed by the specific density ρ with the help of the molecular mass M and Avogadro's number N_A:

$$n = \rho \frac{N_A}{M} \tag{1.19}$$

Introducing the isotopic fraction ϵ_{iso} (49.31% for ^{81}Br), one obtains

$$\frac{dN(Rb)}{dt} = \Phi \cdot \sigma \cdot \rho \cdot d \cdot \frac{N_A}{M} \cdot \epsilon_{iso} \ . \tag{1.20}$$

This equation is valid for a constant α-energy. However, the α-particles lose energy while passing through the bromine target and are stopped finally. Thereby their cross section changes. The target thickness $\rho \cdot d$ per energy is also energy dependent due to the energy dependent stopping power $\frac{dE}{d\rho \cdot d}(E)$. Equation 1.20 can be converted into an integral over the decreasing α-energy:

$$\frac{dN(Rb)}{dt} = \Phi \cdot \int_{E_{min}}^{E_{max}} \sigma(E) \cdot \frac{d(\rho d)}{dE} dE \frac{N_A}{M} \cdot \epsilon_{iso} \tag{1.21}$$

A detailed simulation using the NIST energy loss tables [17] yields the following results for particles with a primary energy of 54 MeV (see figure 1.9, top). After losing slightly less than 10 MeV by passing through a 100 μm aluminum foil, separating a water cooled ampule from the accelerator vacuum[4], 100 μm water and 200 μm SiO_2, the particles enter liquid bromine with an energy of 45.4 MeV in the center of the quartz tube, where they travel 1 mm before they are stopped. A comparison to figure 1.10 shows that for these particles the whole peak of the cross section function is optimally covered. The energy loss increases for particles entering the target off center (see figure 1.9, top). Due to the curved ampule wall the layer of cooling water between the Al window and the ampule becomes

[4] more comprehensive description on the production process is given in the next subsection

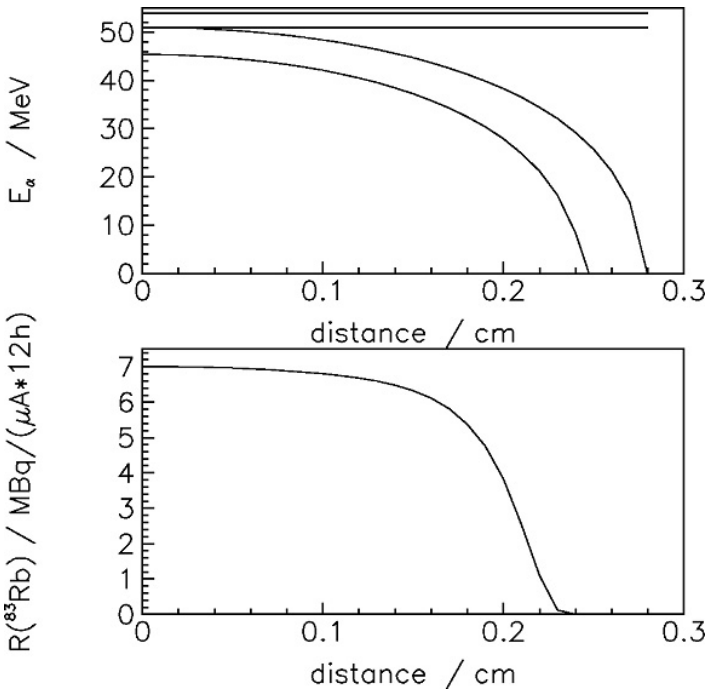

Fig. 1.9: Top: Energy of α-particles at different penetration depth of the target in dependence on the centrality of hitting the quartz tube. Top line: primary α-energy, second top line behind the aluminum window, third line after going through water, fourth line: behind the quartz tube which corresponds to the α-energy when entering liquid bromine. Bottom: ^{83}Rb yield using the α energy simulations and the energy-dependent cross section of Thümmler [36].

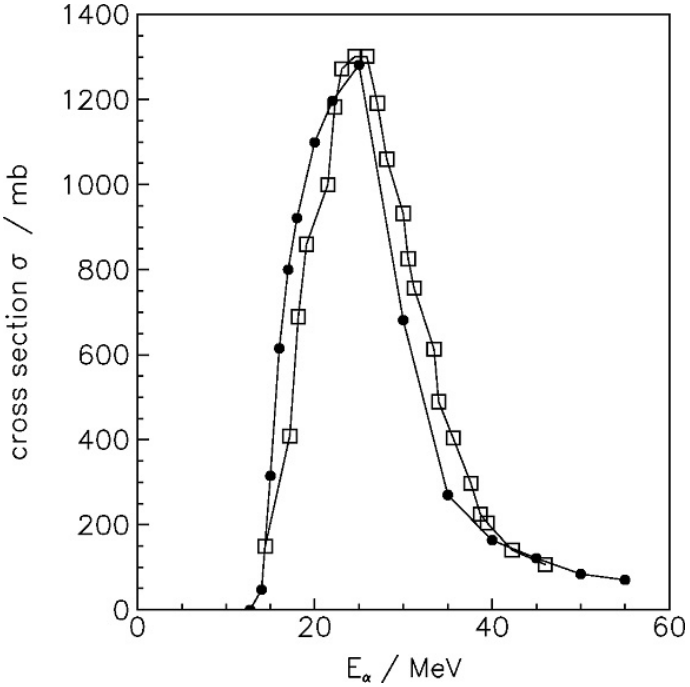

Fig. 1.10: Energy dependence of the ^{81}Br(α, 2n)^{83}Rb reaction cross section from JENDL (closed circles) [18] and from Levkovskij (open squares) [19].

thicker and also the length of the path through the ampule wall increases. The simulations show, that up to a distance of 2 mm from the center line the energy remains high enough (see figure 1.9, top) to cover a sizable part of the excitation function in the bromine target. Inserting the parameters

$$\begin{aligned} \Phi &= r_{target} \cdot 3.1 \cdot 10^{11} \ \frac{\alpha}{s}, \\ N_A &= 6.022 \cdot 10^{23}\,\mathrm{mol}^{-1}, \\ M &= 79.904\,\mathrm{g/mol}, \\ \epsilon_{iso} &= 0.4931, \\ E_{max} &= 45.4\,\mathrm{MeV} \end{aligned}$$

and numerical integration of the cross section $\sigma(E)$

$$\int_{E_{min}}^{E_{max}} \sigma(E) \frac{d(\rho d)}{dE} dE = 150 \frac{mb\ g}{cm^2} = 1.50 \cdot 10^{-25}\ g \tag{1.22}$$

which corresponds to the kinetic energy of alpha particles (see figure 1.10), in the equation 1.21 one yields

$$\frac{dN(Rb)}{dt} = r_{target} \cdot 1.5 \cdot 10^{8}\ s^{-1}. \tag{1.23}$$

Using the total irradiation time of $t = 600$ s and the half-life of ^{83}Rb of $T_{1/2} = 86.2$ d one expects a total ^{83}Rb decay rate of

$$N(Rb) = \frac{dN(Rb)}{dt} \cdot t \cdot \frac{ln(2)}{T_{1/2}} = r_{target} \cdot 8.4 \cdot 10^{3}\ \mathrm{Bq}\ . \tag{1.24}$$

The large maximum cross section of $\sigma = 1300$ mb at a particle energy of 26 MeV (see figure 1.10), using this formula, a ^{83}Rb production rate of 0.58 $\frac{\mathrm{MBq}}{\mu\mathrm{Ah}}$ is expected for central α-rays. This yield drops rapidly for α-rays hitting the quartz tube off-center more than 0.15 mm. (see figure 1.9 bottom).

Sample preparation

Approximately 3 cm^3 of natural liquid bromine assay (99.5% purity) was filled into a quartz tube (6 mm outer diameter with 200 μm wall thickness and 80 mm

length). Afterwards the tube was inserted in a prepared bore of a cylindrical copper platform. The platform was pre-cooled by sinking it into liquid nitrogen. It caused the bromine to freeze, which reduces a risk of human injury. The top of the tube was closed using hydrogen or acetylene burners forming an ampule. As a result of the described actions, some water could have been condensed inside on the tube walls. The remaining volume of the sealed tube contained ambient atmosphere. The tube was placed in a target holder made of acrylic glass with the front beam window made of aluminum foil (thickness 100 μm). The window separates the water cooled setup from the cyclotron vacuum. Thus, in the center of the tube a layer of approximately 5.6 mm of liquid bromine was hit by the beam. A constant flow of demineralized water from the back provided the necessary cooling of the quartz tube. To avoid contamination of the primary cooling cycle with radioactive bromine (in case of cracks on the surface of the tube) a second closed cooling cycle constructed from glass was installed. A video camera, focused on the lateral side of the transparent acrylic glass target holder, was used to adjust the beam according to the fluorescence of the α-particles hitting the quartz ampule. The same principle was applied for the beam ingress monitoring. The central positioning of the beam at the beginning of the irradiation was adjusted on another camera focused on the so called a "blind" window. The blind window is a window made of quartz placed in the monitor beam, a fluorescent track of the window allows beam positioning observation. After the adjustment the window is removed from the beam path.

To study the efficacy of the setup and the stability of its components under irradiation, eleven tests irradiations with beam current and irradiation time variation were carried out. Average currents were in the range between 300 and 800 nA, a maximum irradiation time of 60 h was reached (Table 1.3). Activity of the samples was determined by estimating area under ^{83}Rb peaks at 520.4 keV, 529.6 keV, and 552.6 keV. An inter-comparison of the gained radioactivity with the yield calculated above, shows that only between 33% and 88% of the theoretically achievable activity has been produced. This is due to instabilities in the beam position and deviations from the ideal beam profile assumed for the calculations.

In the further production experiments, a maximum beam current of 1μA was

No.	Average beam current [nA]	Current integral [μAh]	Activity of the closed target [MBq]	Activity after the Br evaporation [MBq]	Fraction of the theoretical yield
1	300	1.8	0.43	0.43	41%
2	500	6.5	1.26	1.26	33%
3	500	13.8	5.49	5.49	68%
4	800	45.0	18.0	18.0	69%
5	350	N/A	–	1.7	N/A
6	400	N/A	–	0.3	N/A
7	450	N/A	–	0.001	N/A
8	700	11.9	–	6.09	88%
9	300	13.4	–	3.5	45%
10	300	6.3	–	1.6	44%
11	400	17.8	–	6.7	65%

Tab. 1.3: Details of the first eleven ^{83}Rb production runs. After the 4^{th} irradiation no comparison of the activity of the open and closed targets were performed. In case of the 5^{th} and 6^{th} irradiations no information about the charge is available due to malfunctions in the integrator. Accidentally, the sample # 7 was irradiated with deuterons.

used. Thus, an energy of 54 W is deposited in the target, which is within the limits of the water cooling circuits capacity. After the irradiation, the samples were stored for three days. The main competing reactions and the resulting isotopes are listed in table 1.4. The ^{83}Rb and ^{84}Rb activities should be considered in a further period of a week, the short-lived activities are negligible, figure 1.11, 1.12. The top of the quartz ampule was opened by breaking it, the excess bromine fumes flushed out with air flow by passing through a sodium-thiosulfate solution for 72 hours:

$$5H_2O \; + \; Na_2S_2O_3 + 4Br_2 \rightarrow 2H_2SO_4 + 2NaBr + 6HBr \qquad (1.25)$$

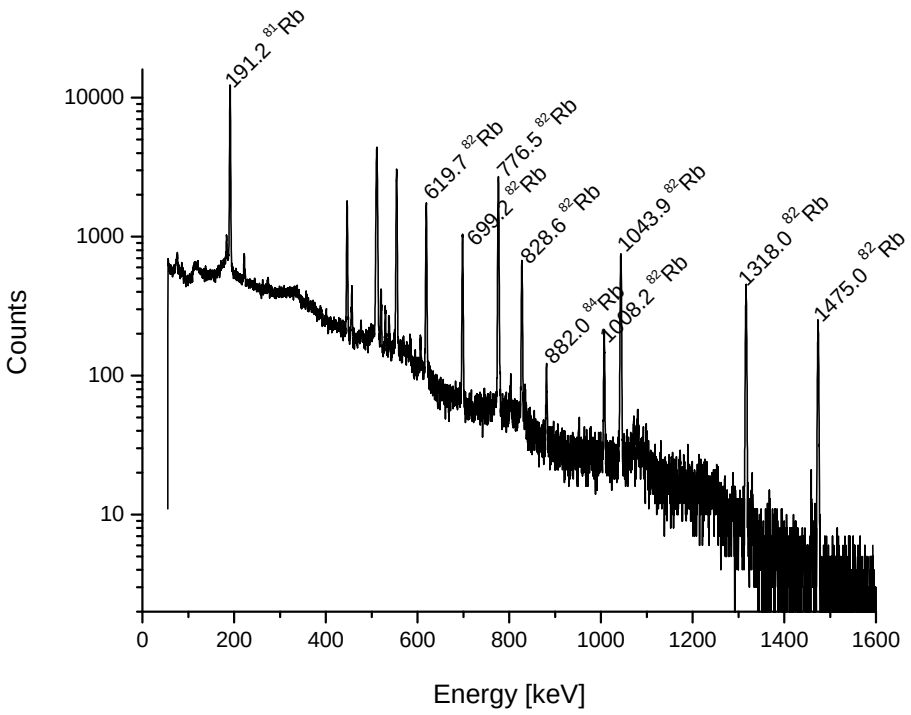

Fig. 1.11: γ-spectrum recorded three days after the end of the irradiation.

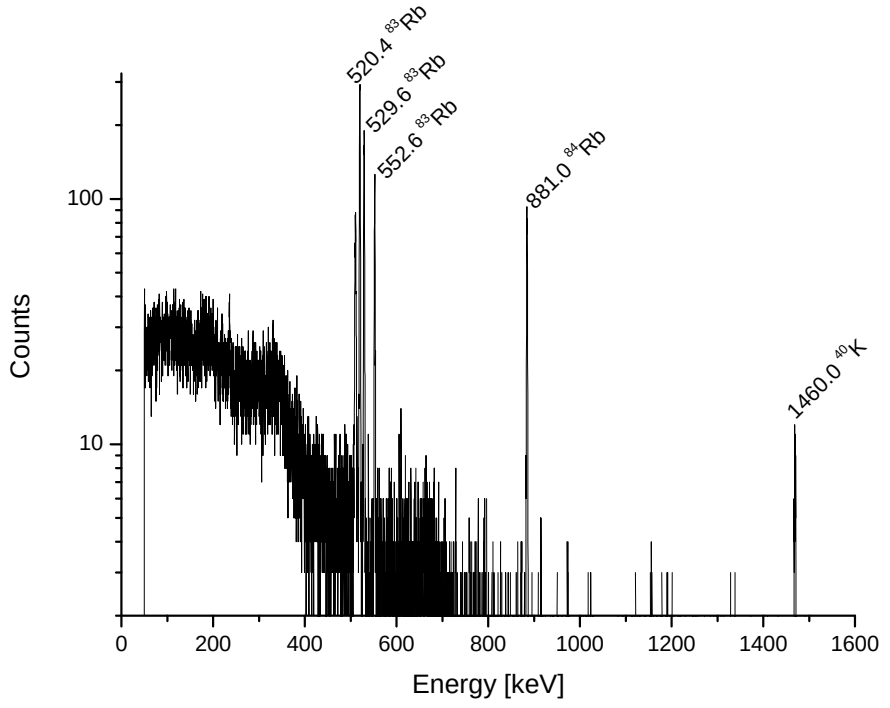

Fig. 1.12: γ-spectrum recorded seven days after the end of the irradiation. Long lived Rb isotopes ^{83}Rb and ^{84}Rb are present.

Product isotope	**Target isotope**	**Reaction**	$T_{1/2}$	**Activity at $t = 0$ [MBq]**	**Activity at $t = 168$ h [MBq]**
^{81}Rb	^{79}Br	(α, 2n)	4.58 h	1070	≈ 0
^{82m}Rb	^{79}Br	(α, n)	6.2 h	1160	≈ 0
	^{81}Br	(α, 3n)			
^{83}Rb	^{81}Br	(α, 2n)	86.2 d	4.9	4.9
^{84}Rb	^{81}Br	(α, n)	32.9 d	1.7	1.7

Tab. 1.4: Comparison of the activity and half-lives of the produced isotopes.

The resultant solution may be disposed of safely. The tube's γ-spectrum was recorded using a germanium detector at different time intervals after the end of the irradiation. A comparison of the spectra of the empty quartz ampule with the filled one showed, that the ^{83}Rb and ^{84}Rb activity had remained completely inside the tube as expected, table 1.3, presumably in the form of rubidium bromide.

1.3.2 Release of ^{83m}Kr

For the planned applications in the KATRIN spectrometers the ^{83m}Kr has to escape from the opened tube and diffuse to the front layer of the condensed krypton source. Therefore, its release from the Rb, stuck to the wall of the tube, was examined in a set-up sketched in figure 1.13. The ^{83}Rb containing tube was placed in a metal container on the left hand side of the figure. The container was connected through a flexible tubing to a closed cycle refrigerator unit (Displex, Oxford Instruments [42]). A copper foil was wrapped on a cold finger over a temperature-sensor-diode. An acrylic glass cap served as a vacuum shield, at the same time remaining transparent for X-ray radiation. The valve to the ^{83}Rb source was opened, and the whole system was evacuated to a pressure of the order of 10^{-5} mbar for insulation, and to avoid humidity and gas condensation on the inner surface of the setup. Subsequently, the refrigerator unit was engaged to cool the cold finger down to approximately 20 K. Thus, any Kr atom released from the source could diffuse through the pipe, and after passing a nozzle condense on

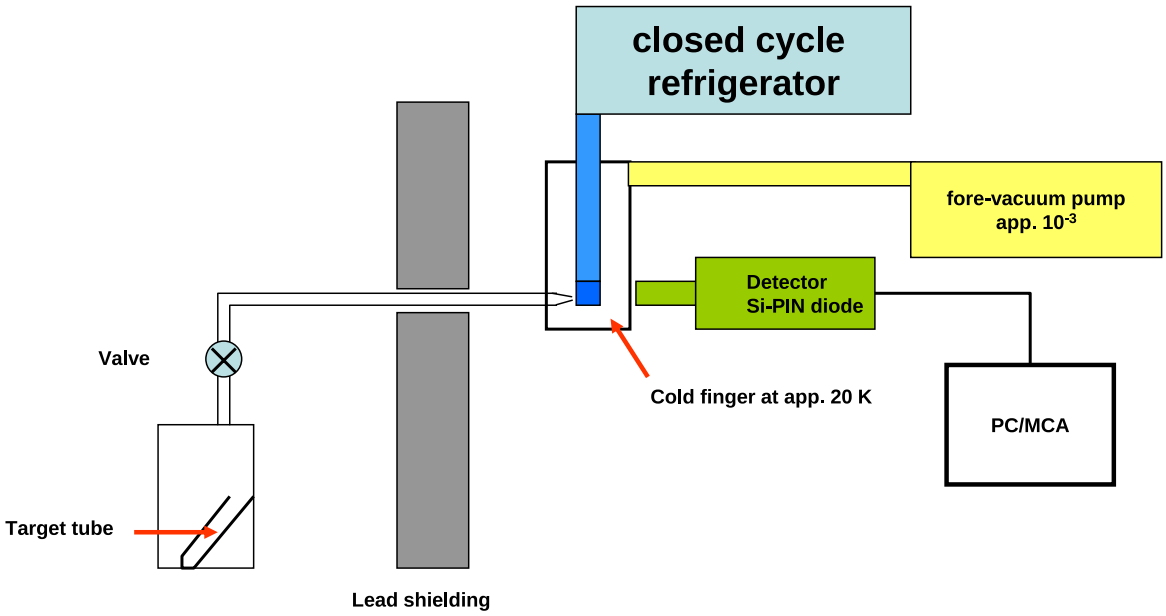

Fig. 1.13: Schematic of the setup for the detection of Kr release from the ampule. The ^{83m}Kr/^{83m}Rb tube is pointed with the red arrow.

the cold finger surface. However it is possible that the krypton could get stuck to other cold parts of the unit.

The presence of the adsorbed ^{83m}Kr on the cold finger was observed with an Amptek^{TM}Si-pin X-ray diode placed in front of the acrylic glass cap. The diode was calibrated with two X-ray (13.95 keV and 17.74 keV) lines from a ^{241}Am source. Krypton spectra were taken for 100 s periods at regular intervals of 25 min. Due to the low efficiency of the pin diode for radiation of higher energy (more than 40 keV) prior to cooling no counts were observed in the 30 s measuring interval. However, as soon as the temperature of the cold finger dropped below 200 K the detector began to record events. A characteristic X-ray spectrum of the ^{83m}Kr with three pronounced peaks is shown in figure 1.14. The peak at 9.41 keV is due to the lowest nuclear transition of ^{83m}Kr (see figure 1.15). The peaks at 12.63 keV and 14.6 keV are due to the K_α and K_β X-rays emitted after the 32 keV conversion electron decay respectively.

The count rate stabilized as the equilibrium state between the release rate from the source and the decay rate of the condensed ^{83m}Kr activity was reached. Taking into account the efficiency of the pin diode for the 12.6 keV line (70%) and a measured transmission of the acrylic glass window ($T = 66\%$) a total efficiency

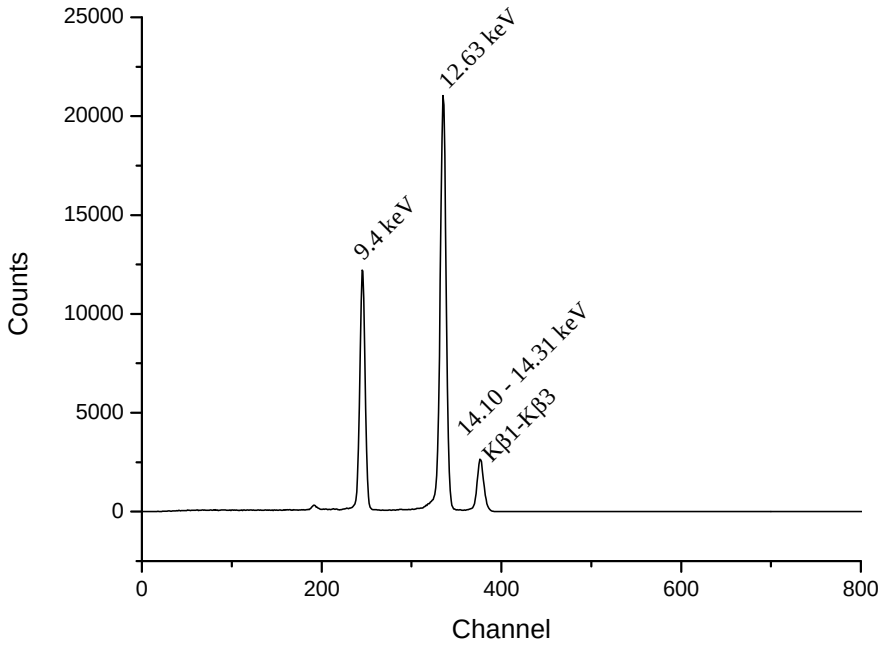

Fig. 1.14: A characteristic X-ray spectrum of ^{83m}Kr.

of 46% is calculated. With this value it was estimated that in equilibrium ^{83m}Kr with an activity of 13 kBq was trapped on the cold finger.

In a further test the valve to the ^{83m}Kr generator was closed, and the decay of the activity captured on the cold finger was monitored. As shown in the figure 1.16 fitting the data yielded a half-life of 1.84(23) h, which is in agreement with 1.83(2) h - the value given in the reference literature.

As a check to prove the complete release of krypton from the generator ampule, the concentration of gaseous ^{83m}Kr was measured in a known volume. An ampule containing ^{83}Rb activity of 66 kBq was placed at one end of a plastic tube, 43 cm long, with an outer diameter of 10 mm and 1.5 mm wall thickness. Then both ends of the plastic tube were plugged. The plastic tube was left for 24 h to let activities of the both isotopes reach equilibrium. After that several points along the tube were scanned with the XR100CR detector for counts under the 12.6 keV peak of ^{83m}Kr. The result is shown in figure 1.17. To calculate the activity in the gas volume it was assumed that, after reaching equilibrium, a ^{83m}Kr activity of 66

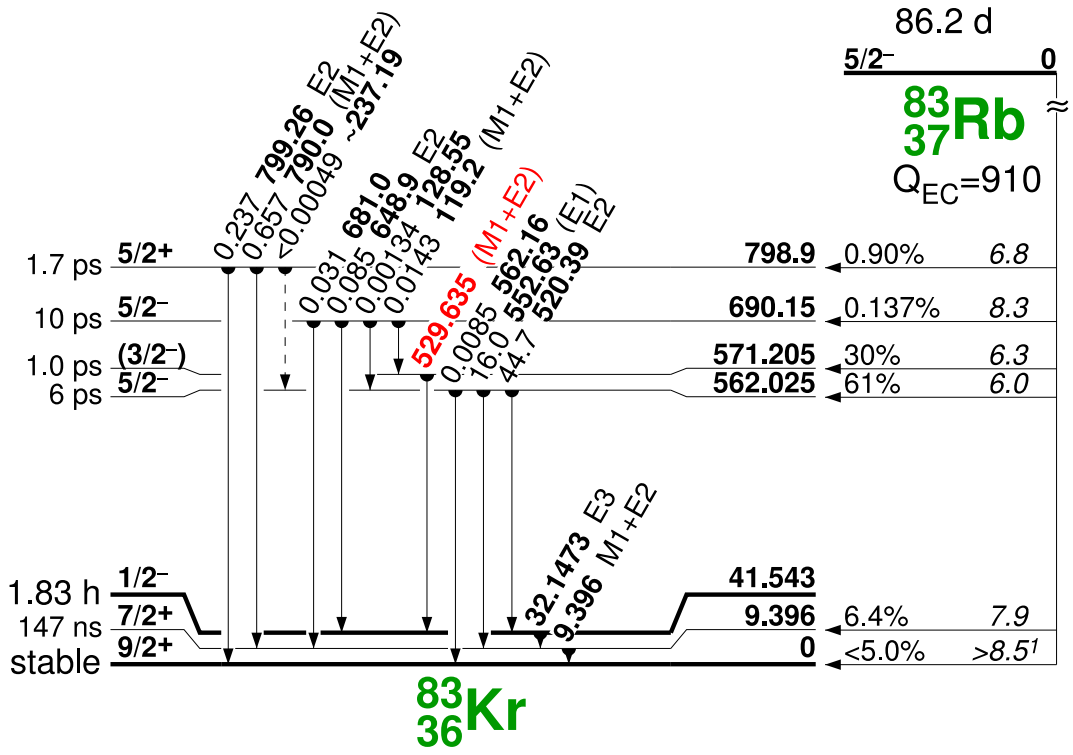

Fig. 1.15: ^{83}Rb/^{83m}Kr decay diagram. [34]

kBq is homogeneously distributed in the tube leading to a volume concentration of approximately 4 Bq/mm^3. The part of the tube near the pin diode is then divided into imaginary cubes of 1 mm^3 with an activity of $A_i = 4$ Bq assumed to be concentrated at centre of the each cube. One cube contributes with C_i the number of counts recorded in the time interval t, b the branching ratio (17 %), the efficiency of the detector (70%), and T_i the transmission factor for the tube walls. The solid angles and the effective transmission T_i for every cube within a volume of ± 30 mm from the position of the detector geometrical center were calculated. Previous tests with the 13.95 keV line of a ^{241}Am source had shown that due to the shape of the housing of the pin diode quanta from larger distances were not registered. Solving the known equation for the activity determination for counts and summing over all cubes yields

$$C_{total} = \sum C_i = \sum A_i \cdot \epsilon \cdot t \cdot \frac{\pi r^2}{4\pi R_i^2} \cdot b \tag{1.26}$$

C - Counts

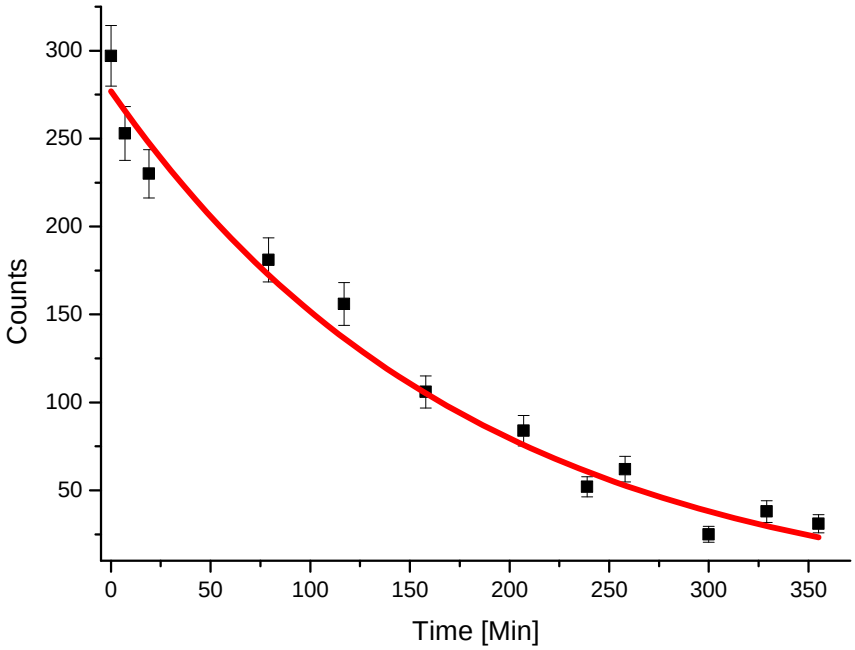

Fig. 1.16: Release of ^{83m}Kr from cold finger.

T - X-ray transmission of the corresponding photon energy for air
ϵ - efficiency of the detector for the corresponding energy
t - measurement time
πr^2 - area of the detector, 7 mm^2
R - distance between the radioactive source and the detector
b - branching ratio
a value of $C_{Total} = 400$ for $t = 600$ s, which is in agreement with the mean value of 350(20) c/600 s found in the experiment (Figure 1.17). The large increase of the values on the right hand side of the plot is due to ^{83}Rb activity concentrated in the ampule close to the wall of the tube. Irradiation of other Br targets led to lower count rates. In some cases however, the measured release of ^{83m}Kr into the gas volume was less than the expected value.

Afterwards the evaporation of the Kr from the cold finger was studied. The system was evacuated again. After the activities reached an equilibrium, the valve to the source was left open, then the cooling unit was switched off. The

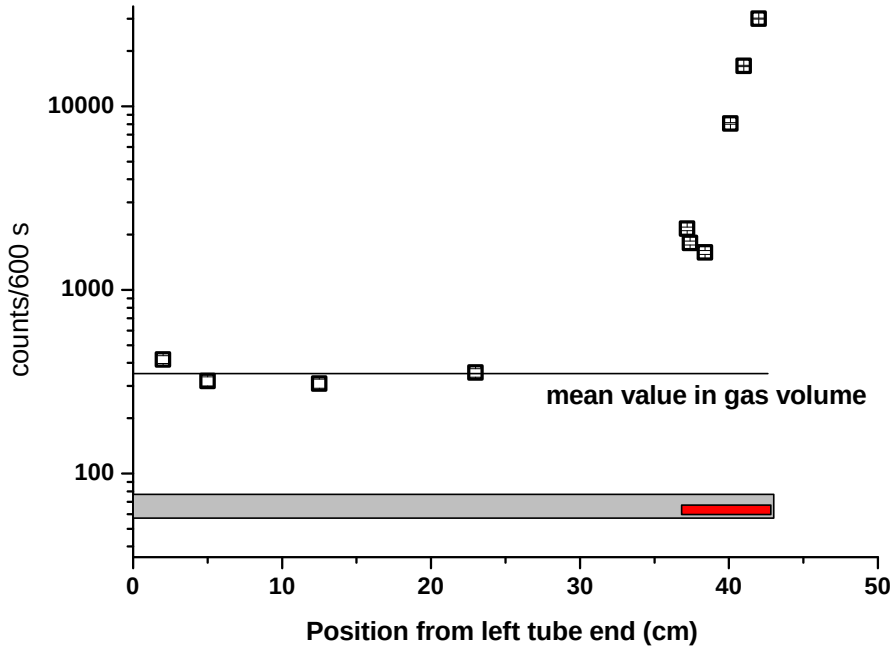

Fig. 1.17: Scanned count rate at the surface of the plastic tube, the ^{83}Rb tube is marked red.

warming up of the cold finger was monitored by a thermo diode. In figure 1.18 the count rate of the 12.63 keV line is plotted versus the temperature. Two strongly marked steps in the count rate are evident: a first one at 100 K and a second around 165 K. From the total ^{83m}Kr activity of 66 kBq it can be calculated that the total number of Kr atoms in the recipient is approximately 10^9. Since a monolayer of Kr adsorbed on the Cu catcher would contain approximately 10^{14} atoms it is clear that the bulk properties of elemental Kr such as the melting point of 116.6 K or the boiling point of 119.7 K are irrelevant for the behavior of the trapped Kr atoms. Instead the adsorption of isolated krypton atoms on copper will govern the adsorption and desorption of Kr. Seyller et al. [44] studied the interaction of Kr with clean, single crystalline Cu surfaces and found that at the lowest pressures Kr started to be adsorbed at 48 K. Therefore, the shift of the first desorption step to 100 K is most probably due to the interaction of residual impurities on the copper surface with the adsorbed Kr atoms. The second, slightly less pronounced step at 165 K may be due to the release of Kr,

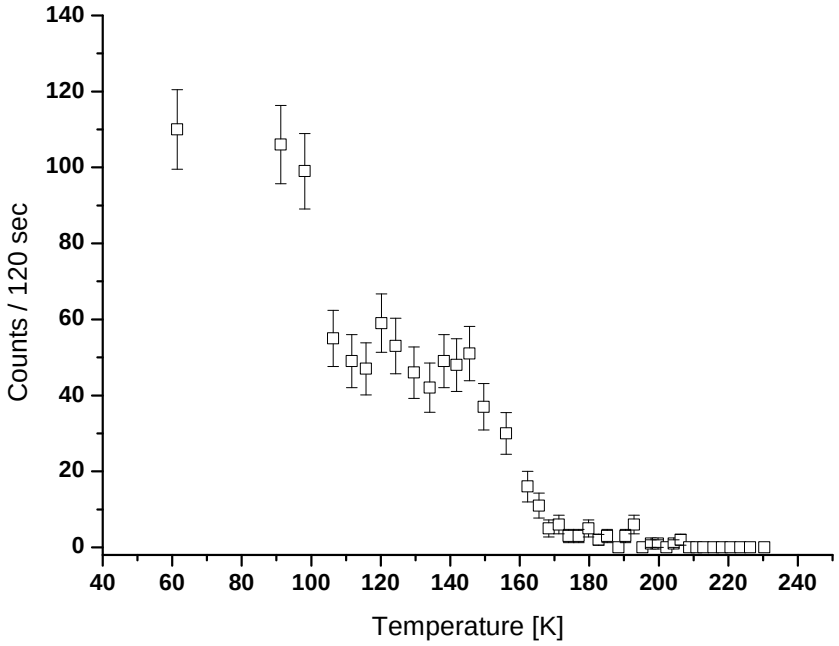

Fig. 1.18: Count rate observed in Kr evaporation from cold finger surface.

previously trapped in a matrix of another gas condensed on the cold finger from the residual atmosphere in the vacuum chamber (Also it is possible that the surface temperature differs from the temperature registered by the diode). The most probable candidate is CO_2 with a sublimation point of 195 K.

In the case of any ^{83}Rb activity escaping from the irradiated ampule, contaminating the spectrometers, it may lead to high background within due to its long half-life. Therefore, after running the experiment for seven days and a subsequent warm up of the cold finger the copper foil used as trapping shield was removed and placed in front of the germanium detector. In a background corrected spectrum taken for 12 h no trace of the characteristic lines of ^{83}Rb could be observed. So, any contamination of the spectrometer with Rb isotopes can be excluded.

Temperature dependence of the ^{83m}Kr release

Already first trials with the CKrS and the monitor spectrometer pointed to a deficit of the ^{83}Kr release from the ^{83}Rb tubes produced at Bonn University [46]:

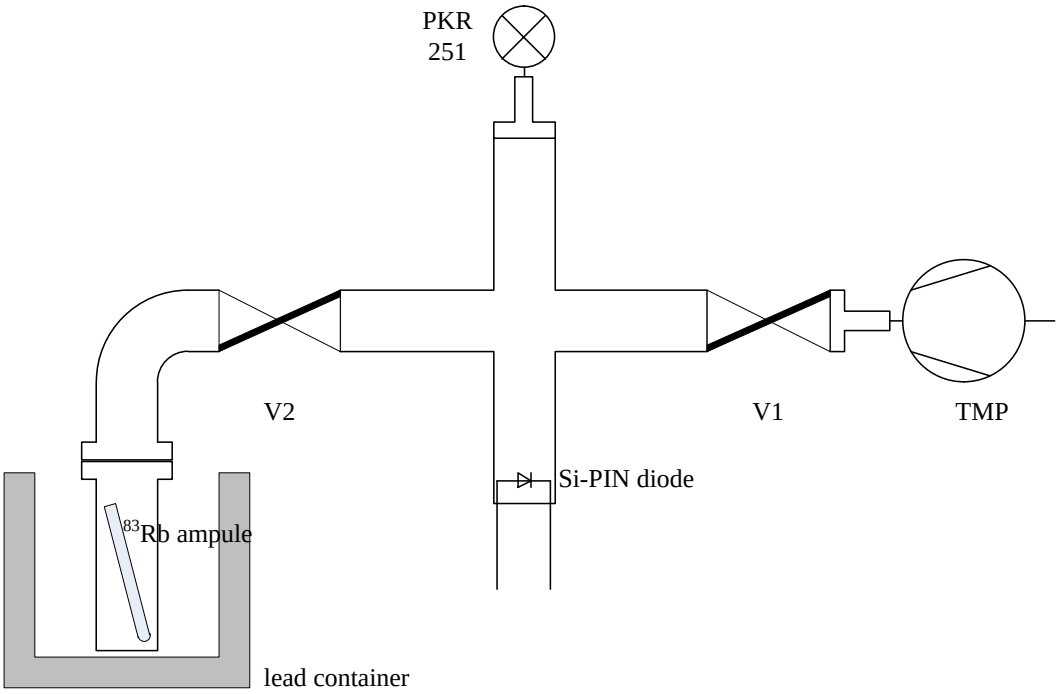

Fig. 1.19: Schematic drawing of the set-up. V1, V2 – valves, PKR 251 – a vacuum gauge, TMP – turbo molecular pump, Si-pin – Silicon photodiode, ^{83}Rb – an ampoule with the ^{83}Rb/^{83m}Kr generator inside a steel container. A band wrapped around the steel container, power supplies and temperature resistors are not shown.

^{83}Rb activity was found by 520 keV, 529 keV and 550 keV γ-lines registration with a germanium detector. Then the 32 keV electron line from a frozen ^{83m}Kr on a high oriented pyrolite substrate placed in front of the monitor spectrometer was registered by a Si-pin diode. A low count rate of the ^{83m}Kr pointed to the fact that there was a deficit of the ^{83m}Kr activity in the gas phase at equilibrium of two isotopes. There was an assumption that the deficit in release is due to humidity accumulated in the process of welding of the quartz ampule using a hydrogen burner as described in the previous section. An attempt to increase the Krypton release is discussed below.

The setup shown in figure 1.19 was assembled. The 640 kBq radioactive ^{83}Rb source was placed in a stainless steel container. A capillary from a container was connected through a valve, V2, to one of the legs of a vacuum cross. In the other two legs of the cross a vacuum gauge (PKR 251) and a Si-pin diode were installed. The *Hamamatsu* S3590-06 diode has an area of 9×9 mm^2, with a front silicon

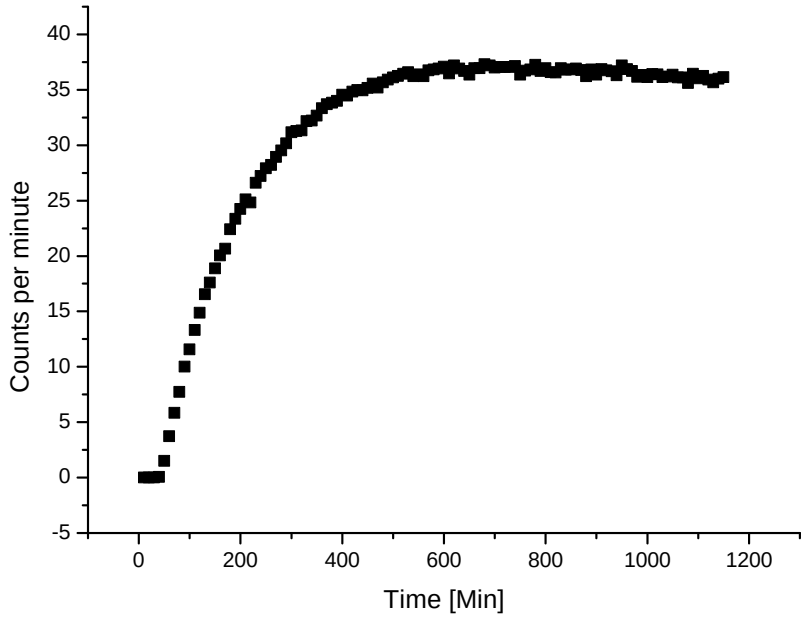

Fig. 1.20: Saturation of the ^{83m}Kr observed in the cross before heating.

window for electron detection. The remaining leg of the cross was connected to a turbo molecular pump (TMP).

Afterwards the whole volume was evacuated with both V2 and V1 valves open. As there was no further decrease of pressure at 3.2×10^{-6} mbar, the V1 valve was closed. The vacuum gauge was turned off, because electrons from its penning trap were contributing to the noise seen by the detector. ^{83m}Kr emanating from the ampule started to fill the cross volume. Continuous observation of the 32-L-M electrons from the ^{83m}Kr was carried out by means of the diode in a measurement sequence. A single measurement of the line took 5 min real time. The observed data was then recalculated in counts per second. Results of the data acquisition set versus time are shown in figure 1.20. In approximately 10 h ^{83m}Kr reaches equilibrium with ^{83}Rb which can be seen from the saturation of the count rate at 25 counts $\cdot$ s^{-1}.

Afterwards, the container was wrapped with a heating band. Input contacts of the heating band were connected to a transformator. Two temperature resistors were installed at V2 valve and inside the heating band wrapping respectively.

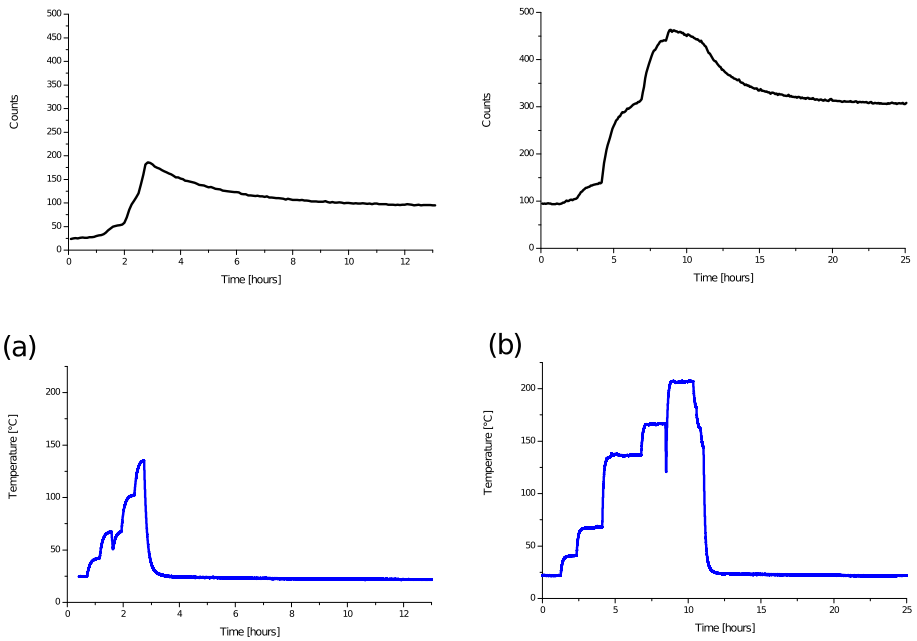

Fig. 1.21: First (a) and second (b) heating experiments' results. The blue curves - behavior of temperature. Solid black curves - behavior of the ^{83m}Kr count rate. Kinks of the blue curve are caused by technical reassembling of the power supplies.

Their impedances were observed by a LabView [47] interface. The voltage was increased in steps, expecting the stabilization of band temperature. An increase of temperature is shown as a blue curve in the figure 1.21 (a), it is interesting that the count rate increased with the increase of temperature (black solid curve). In three hours the count rate yielded 180 counts $\cdot$ s^{-1} at 140 °C. After that the voltage was turned slowly down to zero, however the count rate saturated at the new level of 100 counts $\cdot$ s^{-1} at room temperature.

The voltage was then increased in steps reaching the maximum of 90 V, resulting in a temperature of 216 °C. The count rate continued to raise with the temperature increase. At temperature maximum the count rate showed 490 counts per second (figure 1.21 (b)). Again the voltage was decreased to zero. Also in this case the count rate saturated at a new level of 309 counts $\cdot$ s^{-1} at room temperature.

It is possible that the increase of the count rate was caused by an evaporation of the ^{83}Rb in the volume of the cross, with further contamination of its inner surface. If this were the case, after the closure of V1 a saturated value of the

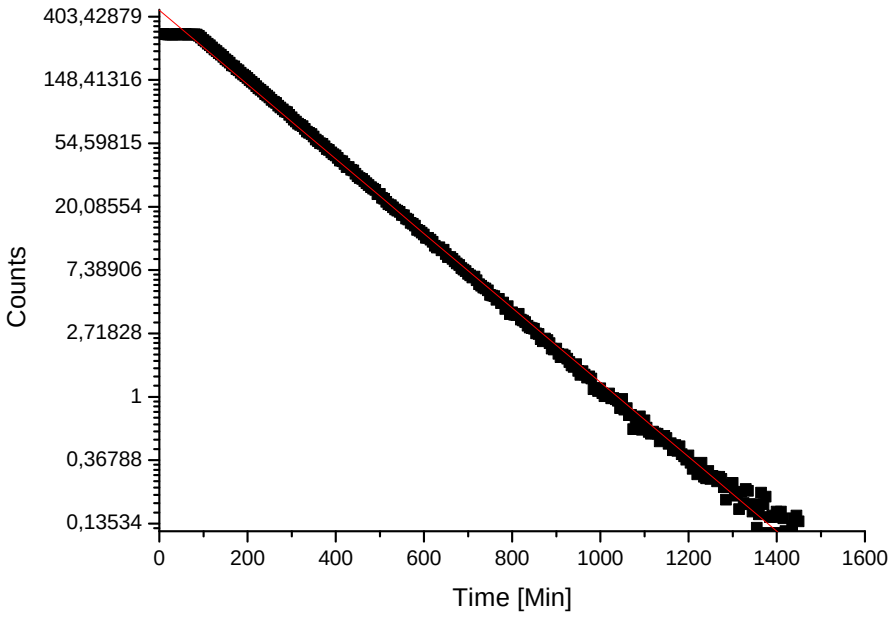

Fig. 1.22: Decay of ^{83m}Kr observed in the closed cross.

^{83m}Kr would be observed. However, after this had been done a decay of ^{83m}Kr gas residue was monitored (figure 1.22). An exponential fit of the decay with 1.84 h is in agreement with the 1.83 h half-life of ^{83m}Kr.

As a last step the volume was once more evacuated to a pressure of 3.2×10^{-6} mbar, with both V1 and V2 valves open. Then V1 was closed, the ^{83m}Kr refill of the volume was monitored. The count rate saturated in 10 h. Interestingly the count rate remained at 301 counts $\cdot\, s^{-1}$ at room temperature. This is 12 times more than the value obtained before the heating procedures.

The increase of the krypton release rate with the increase of the temperature could result from a humidity flush from the system or re-structuring of the RbBr matrix. However, repeated measurements in Bonn with the similar geometry pointed on a contamination of the vacuum components with ^{83}Rb already at the temperature of the heater of 76 °C. That is why the explanation in the beginning of this paragraph can not be considered as truthful, i.e. increase of temperature can not influence the krypton release rate without the vacuum system contamination with ^{83}Rb.

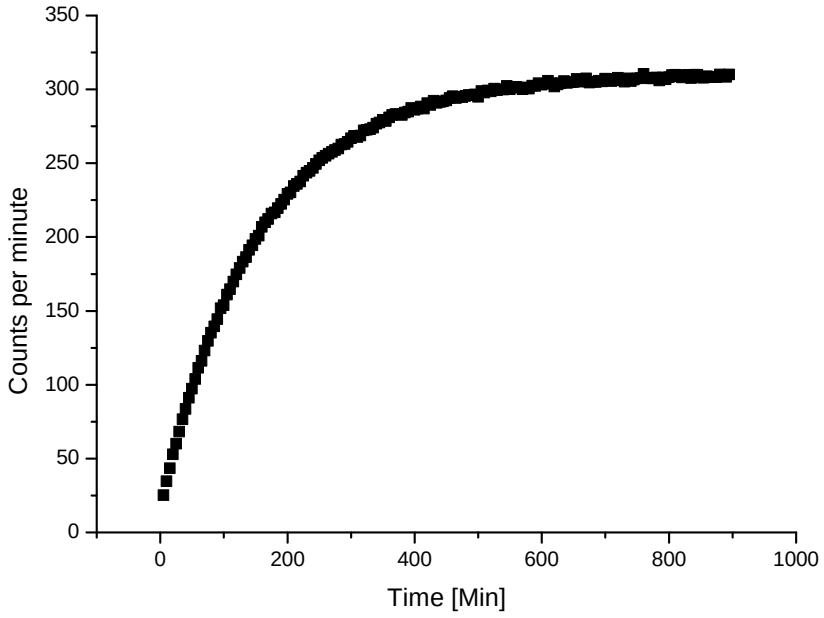

Fig. 1.23: Saturation of the ^{83m}Kr after heating procedures, and re-evacuation of the whole volume.

To eliminate the doubts caused by the complexity of the setups a construction with simplified geometry was presented. The idea of the experiment was to observe the 9.4 keV emission line count-rate from ^{83}Rb alone and count-rate originated from both ^{83}Rb and ^{83m}Kr decays.

A small broken piece of the ampoule with 496(11) Bq ^{83}Rb activity was placed in a bore of 1 mm depth. The diameter of the bore matched the diameter of the XR100CR collimator, 1.9 mm. The detector was placed on the bore. The count rate of 70(10) counts in 120 s was observed under the fume hood. This is 22.4 % of transitions of the ^{83}Rb decay.

Then, a 100 μm aluminum foil was glued onto the bore. It was left for 18 h to get the glue hardening and the isotopes to reach the radioactive equilibrium. 120(10) counts in 120 seconds were observed. Taking into account the 45 % transmission of 9.4 keV for 100 μm Al foil, a count rate of 255(23) counts can be estimated. This is due to 96 % branching ratio in the ^{83}Rb/^{83m}Kr decay.

Since a deviation in the positioning of the detector of 1 mm lead to a con-

siderable error in the activity estimation, it is advantageous to consider the ratio of the observed count rates. It should be equal to the division of the branching ratios 96 %/22.4 % = 4.2. However, the ratio is 255/70 = 3.6, which differs from the predicted number by 14 %. This is due to the systematic errors in the performance of the experiment e.g. mismatch of the detector's geometrical axis with the bore's axis etc. One can conclude that 100 % of the produced ^{83m}Kr is emanated from the RbBr containing ampoules.

Despite of advantages of the CKrS, such as no risk of the monitor spectrometer-contamination, there are disadvantages: repeated condensation of the ^{83m}Kr gas on the HOPG substrate is necessary. A number of time consuming measures before the ^{83m}Kr condensation have to be taken. These are substrate cleaning, its control and ^{83}Kr condensation.

To overcome such difficulties the KATRIN collaboration is interested in the investigation of a ^{83}Rb/^{83m}Kr implanted source. Venos et al. showed that ^{83}Rb trapped in Zeolithe will not emanate into the monitor spectrometer.

An implantation of Rb in a Pt foil with 30 keV ion energy at Bonn Isotope Separator was carried out. Two ^{83}Rb samples from Řež, 5.4 MBq each, were implanted. This resulted in the efficiency of the implantation of 0.15 % and 0.30 % respectively. To raise the efficiency of the implantation the sample holder was provided with a Cu foil wrap. A test implantation of non-radioactive Rb showed that considerable progress in efficiency (38 %) was achieved. Further trials are in progress.

Conclusion

It was shown that the production of ^{83}Rb from liquid, natural Br is feasible at the Bonn Cyclotron. A number of ^{83}Rb/^{83m}Kr generators were produced for test purposes of the University of Münster. The subsequent transformation of an irradiated target into a source, which can be attached to the KATRIN monitor spectrometer has been tested and is a comparably simple process. This is important considering the large amount of activity, which has to be handled in the planned experiments. Finally, it was found that ^{83m}Kr is released completely from the Rubidium Bromide (RbBr) residue retained in the quartz ampule after the evaporation of the excess Br. Surface effects in the capillary of the CKrS play

a major role since the amount of emanated ^{83m}Kr atoms result in a disintegration in the order of 10^6 per second. Improvements of this procedure, like the use of isotopic enriched materials seem unnecessary at the moment since the possible gain of about a factor two compares unfavorably to the cost and availability of the necessary quantities of enriched Br.

A possibility of ^{83}Rb implantation with 38 % efficiency is shown in the example of non-radioactive Rb implantation.

Chapter 2

Isotopes for XRD studies on planets

2.1 Motivation

In situ analysis of regolith and rocks on the planets of solar system was always one of the foreground scientific directions of space exploration missions. Search for water or complex organic molecules can be interesting for astrobiology and astrogeology. Their presence can point on formation of early forms of life, throw light into mineral formation. Until the last decade mainly topological studies were made with optical equipment in visual range. The priorities are now at geological and mineralogical methods, such as X-ray diffractometry (XRD) as a tool for crystallinity study and X-ray fluorescence for elemental composition (XRF).

Space missions have strong restrictions on the mass and power consumption of the experimental equipment. That is why utilization of a microfocus X-ray tube is unfeasible. A usage of compact, light-weight radioactive isotopes as X-ray sources is considered as an alternative. The half-life of the concerned isotopes must be comparable with the space mission duration of several years. Furthermore, in order to offer optimum conditions for powder diffractometry or fluorescence under the severe restrictions of an exploration mission, a photon flux of more than 10^6 photons per second must be provided. Low flux will increase the measurement time, influencing the consumption of the valuable resources like power and data processing.

Isotopes applied so far ^{55}Fe and ^{241}Am are not optimal for these purposes. ^{55}Fe was exploited in former missions. Having an initial flux of $4 \cdot 10^7$ ph/s, only $7 \cdot 10^6$ ph/s will remain after 5 years. Simultaneously 6 keV X-ray energy does

not help suppressing background prolonging the measurement time. The latter causes increase of power consumption and data transfer.

Commercially available ^{241}Am delivers two X-rays which could be used for diffractometry, with 14 keV (37%) and 60 keV (36 %). A very long half-life of 432.2 years would result in a constant photon flux over a mission duration of 10 years. It can be produced in large quantities, measured in grams, e.g. at Oak Ridge National Laboratory, USA [48]. α particles emitted from the source can be easily shielded, letting X-rays transmit. However, ^{241}Am suffers from a low activity per mass ratio 126 GBq/g. Which is further reduced by a strong attenuation of the 14 keV X-rays in the source body. An estimate for a $5 \times 5 \times 0.1$ mm^3 source gives a flux of $6 \cdot 10^7$ ph/s.

Alternative sources considered here are ^{109}Cd and ^{101}Rd. ^{109}Cd already serves for the terrestrial mobile XRD and XRF measurement kits. ^{101}Rd to our knowledge is proposed for the first time. A study on their production feasibility at Bonn Isochronous Cyclotron has been carried out.

The X-ray diffraction method can be explained on the set-up used at the Technical University of Dresden (TU Dresden) (figure 2.1). An X-ray source is located in a lead box with a collimator for primary axis of the ray. At the other end of the collimator a film with sample is located. A very well characterised diffractometry standard sample Si powder is used: A fine layer of the Si-powder-vaseline mixture is smeared on the plastic film. A Si Drift Detector (SDD) is located on an interface controlled mechanism. After enough experience with the sample is collected, studies with test samples can be started.

The angle between the primary ray and the detector, 2θ, is set by the interface. According to W. L. Bragg [49] constructive interference of the radiation reflected from successive crystal planes occurs whenever the path difference is an integral number n of wavelength λ:

$$2dsin\theta \ = \ n\lambda, \tag{2.1}$$

where d is a distance between a series of parallel lattice planes in an observed crystal.

For a real interplanetary mission it is planned to fix the source and detector on a mobile robotized unit. No foil will be used: The primary ray will be directed

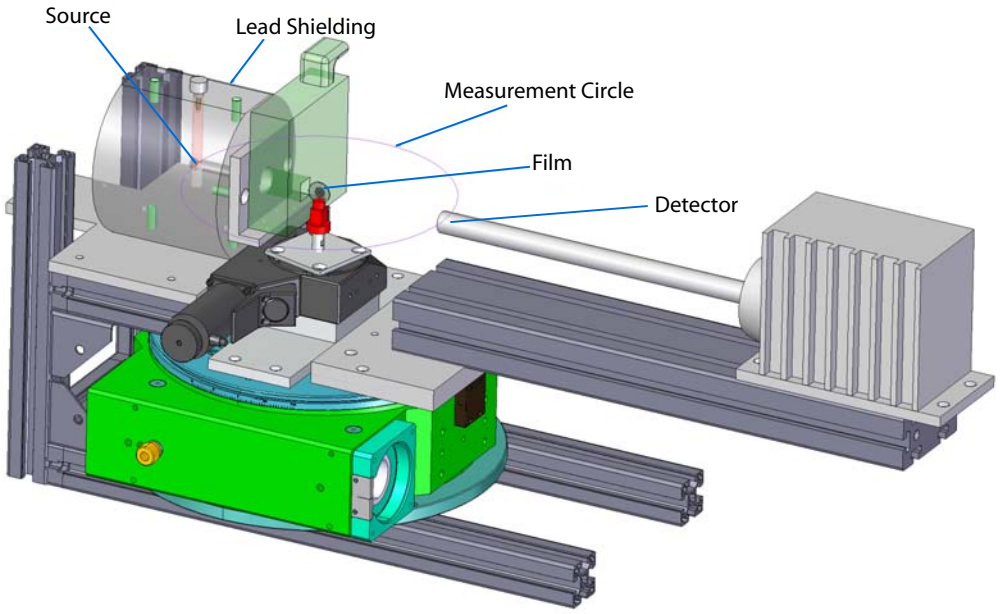

Fig. 2.1: Set-up at the Technical University of Dresden. The radioactive source is placed in a lead collimator box. A film with Si powder is fixed on a stage. The detector mounted on an interface controlled platform can be brought into movement around the measurement circle. (Courtesy of the TU Dresden)

on the surface of the planet, diffracted rays will interact with the detector. Registered events will be recorded by Data Acquisition System, further transmitted with a signal to the controlling unit.

2.2 The isotope ^{101}Rh

^{101g}Rh decays through electron capture into ^{101}Ru with 3.3 years half-life, (figure 2.2), making it an ideal candidate for an X-ray source for interplanetary missions. Its X-ray characteristic lines, 19.15 keV and 19.279 keV, lie in the range especially interesting for X-ray spectroscopy due to successive suppression of background. For runs at Bonn the ^{99}Ru(d, 2n)^{101}Rh production reaction with a high cross section was chosen. Because no cross section data for the reaction

Isotope	**X-rays**	**Emission energy**	**Intensity**
^{101g}Rh	K_{α_2}	19.15 keV	22.8%
	K_{α_1}	19.28 keV	43.0%
^{101m}Rh	K_{α_2}	19.15 keV	17.8%
	K_{α_1}	19.28 keV	34.0%
^{109}Cd	K_{α_2}	21.99 keV	29.7%
	K_{α_1}	22.16 keV	56.0%

Tab. 2.1: X-ray emission lines of ^{101g}Rh, ^{101m}Rh and ^{109}Cd

on ^{99}Ru were available, the one for ^{103}Rh(d, 2n)^{103}Pd was used which has a maximum $\sigma_{\max} = 1200$ mb at a deuteron energy of 13 MeV [38]. Another reaction contributing to the ^{101}Rd production, ^{100}Ru(d, n)^{101}Rh, has a much lower cross section maximum of $\sigma_{\max} = 270$ mb at 9 MeV [38]. For convention the side of the sample, facing the beam was named *front side*. The other side is correspondingly referred to as *rear side*. Due to high self-absorption (the mass attenuation coefficient $\mu/\rho = 14.99$ cm^2/g) for 20 keV X-rays in the ruthenium body, an initial energy value of deuterons were optimized by means of SRIM [41] simulations to maximize the density of activated nuclei in the rear side of the ruthenium sample. Figure 2.4 represents the spacial distribution of ^{101}Rd in the ruthenium sample body for two initial beam energies of 20 MeV and 27 MeV. Table 2.2 presents corresponding yield of 20 keV X-rays from ruthenium samples of different thickness. Transmission probability for the 20 keV X-rays from the front side of the pill is negligible, less than 2%. A 27 MeV beam at 300 μm ruthenium sample thickness was found to be optimal for these purposes, giving an X-rays outcome of about 28%.

A yield prediction, made according to the method introduced on the page 31, led to a tiny value of 0.03 $\frac{\text{MBq}}{\mu\text{Ah}}$ for the ^{101g}Rh. But luckily there is an isomeric state of ^{101m}Rh with 4.34 days half-life, having the same X-ray emission lines (figure 2.3). A comparison of the X-ray intensities of the both isotopes is listed in table 2.1. The ^{101m}Rh yield of 8.7$\frac{\text{MBq}}{\mu\text{Ah}}$ is 290 times the one for the mentioned ^{101g}Rh. For comparison, in 100 h cyclotron run time with 1μA beam current, roughly 3

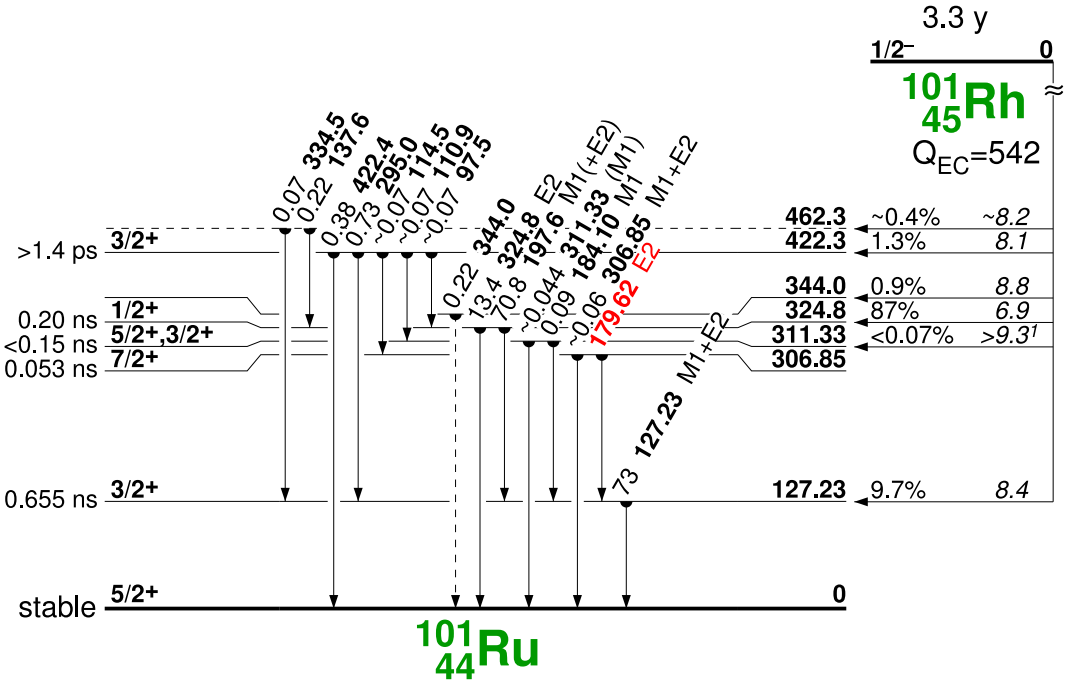

Fig. 2.2: ^{101g}Rh decay diagram. [34]

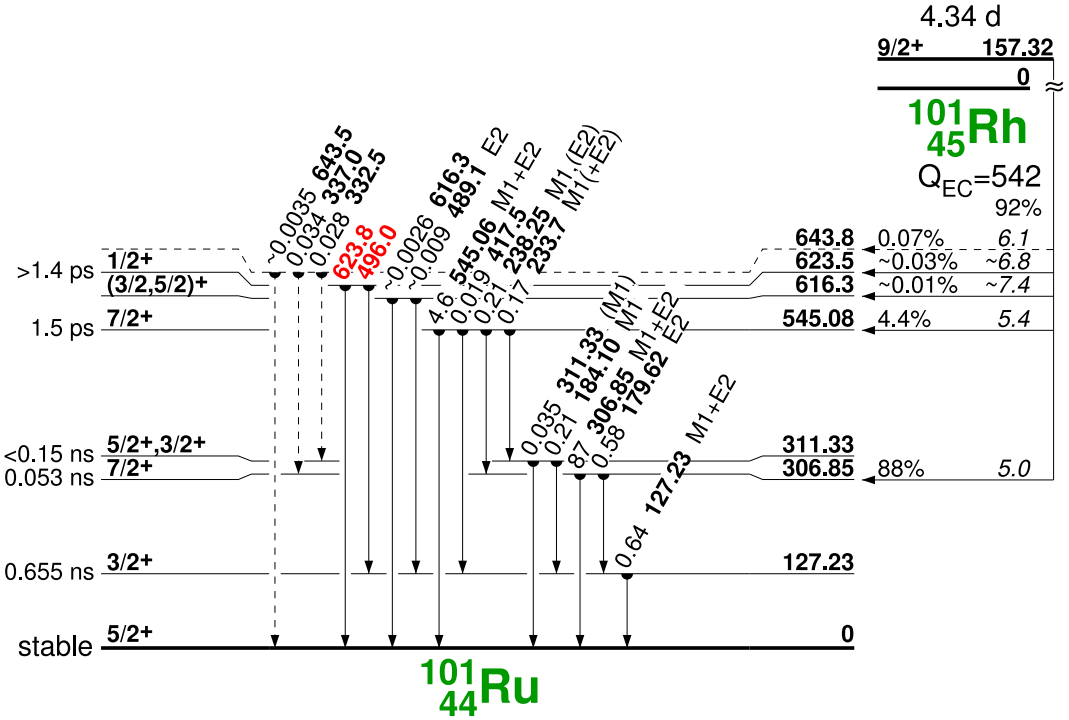

Fig. 2.3: ^{101m}Rh decay diagram. [34]

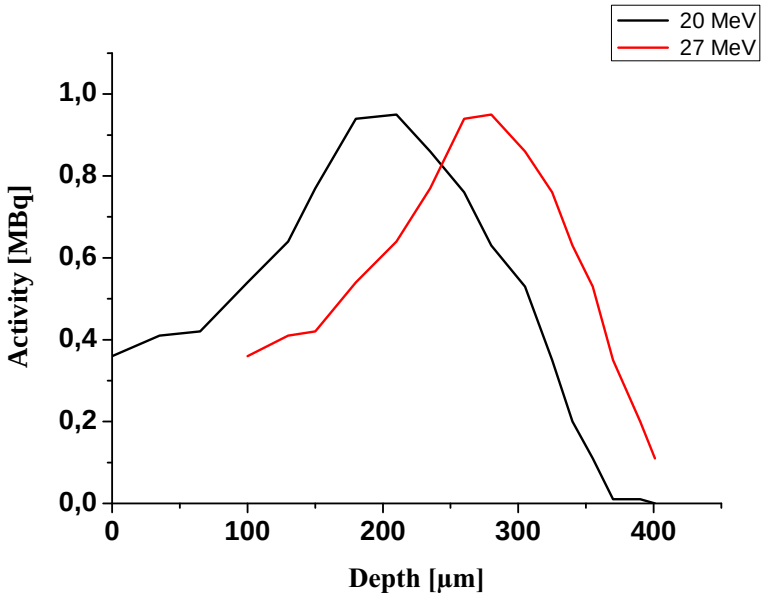

Fig. 2.4: Distribution of the ^{101}Rd with the ruthenium pill's depth at 20 MeV and 27 MeV deuteron beam scenarios.

MBq of ^{101g}Rh and about 900 MBq of ^{101m}Rh can be produced. Of course the short half-life of ^{101m}Rh makes its use for the interplanetary missions unfeasible, but it can be considered for the X-ray diffractometry set-up construction tests carried out by the TU Dresden in charge of EADS Astrium[1]. However, ^{101m}Rh has 306.86 keV with an intensity of 81%. The line can contribute to the Compton background. Experimental estimation of the feasibility of ^{101m}Rh usage for the EADS tests was one of the aims of this thesis. For ^{101g}Rh production for space applications, cyclotrons with higher beam current capabilities such as ISPRA [50], or ZAG Karlsruhe [51] can be applied.

^{101}Rh sample preparation

Natural ruthenium powder (99% purity) was pressed in the form of pills with the maximum last of 32 kN. 5 mm diameter of the pill was set as an upper limit required by the TU Dresden. To estimate the amount of powder necessary for pressing pills of given thickness before pressing them, their volume under given

[1] A daughter company of European Aeronautic Defence and Space Company (EADS) [52].

Initial beam energy	**Ru sample thickness**	**Ratio of emitted Rh X-rays to activity of Rh**
27 MeV	300 μm	27.24%
20 MeV	300 μm	17.66%
20 MeV	400 μm	4.97%
20 MeV	450 μm	2.00%

Tab. 2.2: Expected fraction of Rh X-rays from a pill depending on initial deuteron energy and Ru sample thickness.

diameter D were calculated

$$V = \pi \frac{D^2}{4} d \ . \tag{2.2}$$

Knowing the density of ruthenium, $\rho = 12.6$ g/cm^3, it is easy to find powder's mass

$$m = \rho V \ . \tag{2.3}$$

The mass of the powder was measured with an electronic balance. In fact more amount of the powder was given in the press form, because the first pressure test showed that a residue of the ruthenium powder remains in the form. The masses of the resultant pills were about 0.10 g. The pressed pills were handled with care due to their extreme fragility. The front side surface of the pill was prior marked by scratching with a scalpel (since the sides were not equivalent for emitted X-ray radiation intensity). The pill was placed onto the disk target holder made of aluminum. The top of the pill was covered with a household aluminum foil (15 μm thickness). Flaps of the foil were placed under a grommet with the pill in the grommet's center. The grommet was then fixed with a stainless steel clip. Prior to the irradiation, beam centering trials were performed with paper targets. Afterwards the disk with the sample was placed in the irradiation facility. Water cooling was provided from the backside of the target holder. After the irradiation the pill remained in the facility for three days for short lived activities to decay. Further the holder's coating was removed.

Altogether five sources with varied beam current and irradiation time were

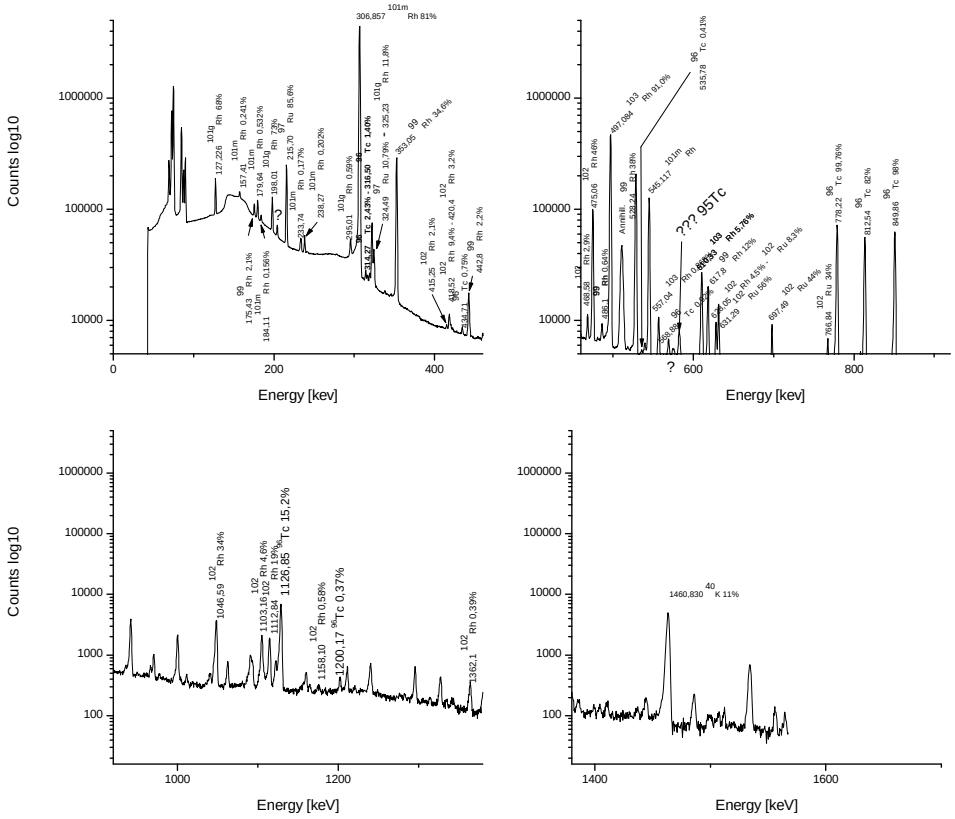

Fig. 2.5: γ-spectrum of ^{101}Rd source.

produced (table 2.3). The first source melted down, due to malfunction of the cooling circuit. Irradiation of the second source was successful. The γ-spectrum of the source is recorded in figure 2.5 with the detailed peak analysis. Since the isotopic abundance of ^{101}Ru is 17%, additional isotopes, ^{96}Rh, ^{97}Rh, ^{98}Rh, ^{99}Rh, ^{100}Rh, ^{102}Rh, ^{103}Rh, ^{105}Rh and ^{96}Tc, with half-lives ranging from 42 s to 2.9 years were produced. These are listed in table 2.4. Among the isotopes to ^{102}Rh attention should be paid. Its isomers have the longest half-lives of 207 days and 2.9 years, resulting in the contribution of its 19.15 keV and 19.28 keV rays in the X-ray spectrum, which is good. However, its high energetic γ-lines, 475.06, 631.29, 697.49, 766.84, 1046.59 and 1112.84 keV, contribute to background. This complication can be eliminated using 100% pure ^{101}Ru powder. A granule of the source was found to be broken out after the end of the irradiation. X-ray

No.	Calculated ruthenium thickness	Beam energy	Current integral	Activity of ^{101m}Rh [MBq]	Activity of ^{101g}Rh [MBq]
1	300 μm	27 MeV	7.5 μAh	Melted	Melted
2	300 μm	27 MeV	1.0 μAh	13.4	0.06
3	300 μm	27 MeV	48.0 μAh	425.0	1.5
4	450 μm	20 MeV	1.0 μAh	8.5	0.03
5	370 μm	19 MeV	140.0 μAh	1200	4.2

Tab. 2.3: Details of the ^{101}Rh production runs.

spectrum of the granule was recorded using an Amptek XR100CR detector, figure 2.6. Neighbouring lines, 19.15 keV and 19.28 keV could not be resolved by the detector. A characteristic line at 20.6 keV corresponding to ^{97}Ru is present. 21.53 keV related to 21.63 keV and 21.66 keV from both ^{101}Rd isomers can also be seen. Further, there is a peak at 6.16 keV caused by X-ray fluorescence in the stainless steel housing of the detector. The predomination of the X-ray count rate from the rear side over the count rate from the front side proves the correctness of the SRIM simulations discussed above.

The second and the third sources were shipped to the TU Dresden one day after the irradiation took place. Measurements showed the activity of the third source 425 MBq of ^{101m}Rh and 1.5 MBq of ^{101g}Rh. The group from the TU Dresden informed about insufficient X-ray activity for the experiments: X-ray transmission values of the second and the third sources deviated strongly from the predicted ratio. The reason for this was investigated; the thickness of the mentioned three sources had not been measured before. But by measuring the thickness of the resultant pills and comparing it with their mass it was possible to derive the real density of the ruthenium powder to be 6.3 g/cm^3, half of the literature value. As a result nominal thickness of the first three pills were 150 μm. That is leading to the error in calculations. To estimate the influence of this effect, powder necessary to produce 450 μm pill thickness was taken, prior making calculations according to expressions 2.2 and 2.3. The resultant thickness was corresponding to 225 μm effective thickness of ruthenium. An initial beam energy

No.	Isotope	Half-lives
1	^{96}Rh	1.5 m / 9.9 m
2	^{98}Rh	3.5 m / 8.7 m
3	^{99}Rh	4.7 h / 16 d
4	^{100}Rh	4.7 m / 20.8 h
5	^{102}Rh	2.9 a / 207 d
6	^{103}Rh	56.1 m
7	^{105}Rh	45 s / 42 s
8	^{96}Tc	4.28 d

Tab. 2.4: Auxiliary isotopes produced during ^{101}Rh production runs and their half-lives.

was also reconsidered to 20 MeV. The activity of the fourth source matched the predicted yield perfectly.

For the last, fifth source a pill with a thickness of 370 μm was pressed (which corresponds to an effective ruthenium thickness of 185 μm). Thus the initial beam energy was scaled to 19 MeV. Within a 140 μA $\times$ h irradiation charge at $2 - 2.5$ μA a final activity of 1.2 GBq was estimated. This source was also shipped to the TU Dresden.

The pills purchased for the shipment were fixed on the stage of a sample holder provided by the TU Dresden using *UHU Alleskleber* glue [56]. The front side of the pill was attached with the glue to the sample holder, because the higher X-ray count rate was expected from the rear side. Prior a few non irradiated ruthenium pills were glued on stages made of similar material (aluminum) to check the sticking ability. It turned out that the setting-up time of the glue lies within 2 minutes.

Unfortunately, trials with the fifth source at Dresden were successful only at primary beam direction. At the other directions Compton edge and background contribution from high energetic lines of ^{99}Rh, ^{101m}Rh, ^{101g}Rh, ^{102}Rh and ^{96}Tc isotopes, due to scattering from the shielding, was high.

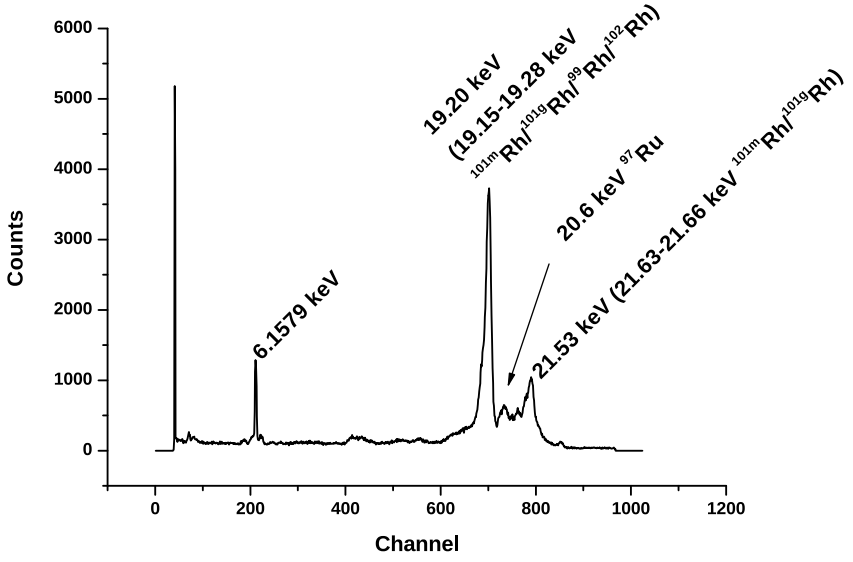

Fig. 2.6: Rhodium X-ray spectrum of the ruthenium pill.

Conclusion

The γ-line of ^{101m}Rh 306.86 keV with an 81% emission probability make a significant contribution to the Compton edge and background. One possibility to solve this problem were letting the ^{101m}Rh to "cool off". Only ^{101g}Rh will remain as a result. However, it is to be expected that this problem will also occur due to the ^{101g}Rh γ-transitions 127.23, 198.01 and 325.23 keV, with intensities of 65 %, 73% and 11.8% respectively which accompany the X-ray emission.

Thus, an application of the ^{101g}Rh is not suited for the X-ray diffraction trials in the set-up version realised in Dresden due to Compton scattering in the collimator and on the structural compounds.

2.3 The isotope ^{109}Cd

The isotope ^{109}Cd has a number of advantages compared to the isotopes mentioned so far. It has a relative long half-life of 462.6 days, as well as only one γ transition at 88 keV (cf. figure 2.7). Due to its low intensity 3.70% and low energy the probability for Compton scattering caused by this line is very small.

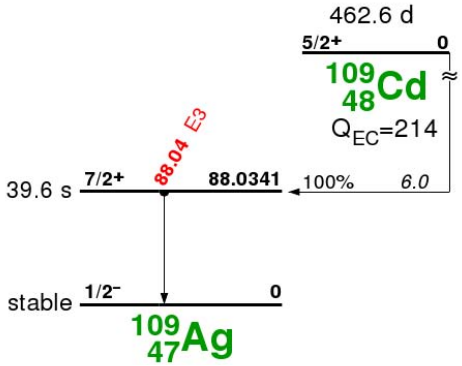

Fig. 2.7: Decay diagram of ^{109}Cd. [34]

Emitted X-rays with energies of 21.99 keV and 22.163 keV and respective intensities of 29.7% and 56.0%, lie like the ones from ^{101}Rh, in the 20 keV range (cf. table 2.1).

As it was mentioned in the previous section this range is attractive due to its background suppression, resulting in shortening of the data acquisition time. The source is widely applied, but no tests for its use in X-ray diffraction in space application instruments has been carried out. An optimization of the source production at Bonn cyclotron has been studied.

A 5×5 mm^2 square plate was cut out of 400 μm thick silver to satisfy the dimension limit set by the Dresden group. The plate contained both isotopes of silver ^{107}Ag and ^{109}Ag, met in nature with abundance of 51.84% and 48.16%. The further handling procedures for the silver plate were similar to the ruthenium pills discussed in the previous section, with a small difference on the initial irradiation energy: 18 MeV – 20 MeV for the ^{109}Ag(d, 2n)^{109}Cd reaction has been applied.

In the case of this source an attempt was made to maximize the distribution in the front side of the target in order to reduce X-ray self-absorption in the silver plate body. The distribution of the ^{109}Cd in the silver plate as a result of 18 MeV deuteron irradiation of latter is depicted in figure 2.8. There is a strong controversy in the cross-section maxima data from different authors. The values range from 400 to 900 mb, forcing yield prediction to vary in between 0.06 to 0.13 $\frac{\text{MBq}}{\mu\text{Ah}}$ [53–55]. That is why a proper judgment without an experimental trial was difficult. An activity estimation made according to 88 keV γ-line using a germanium detector pointed that the yield curve given by Uddin [53] with a

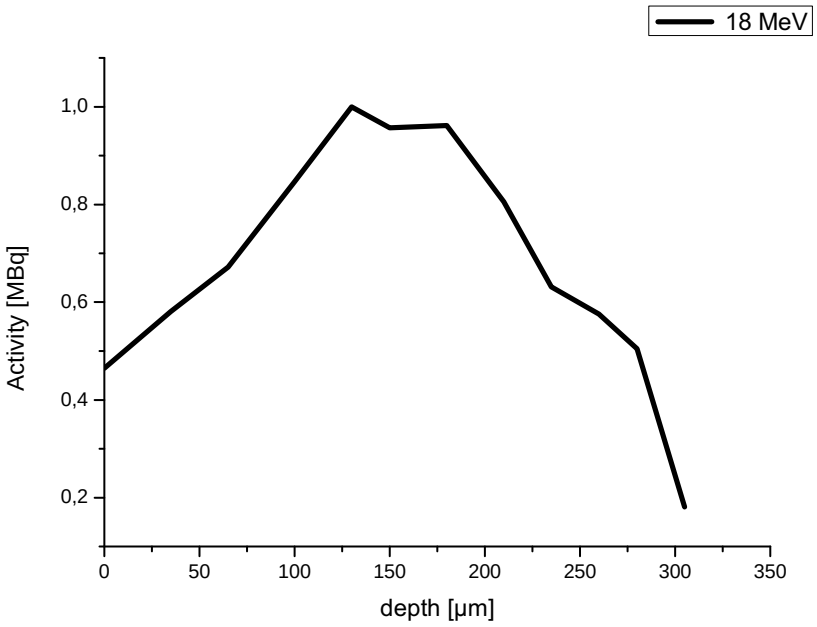

Fig. 2.8: ^{109}Cd distribution in a 300 μm silver foil as a result of 18 MeV deuteron irradiation.

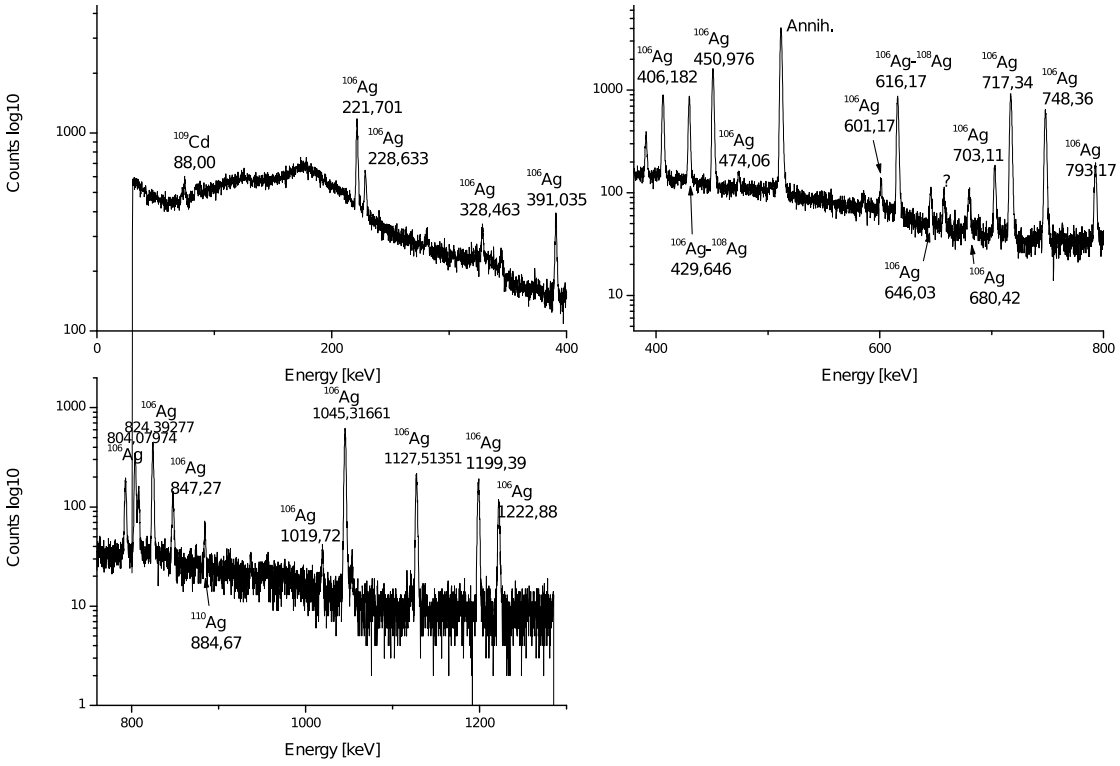

Fig. 2.9: γ-spectrum of the irradiated silver plate.

No.	Plate thickness	Beam energy	Current integral	Activity of the ^{109}Cd
1	400 μm	20 MeV	1.5 $\times$ 27 μAh	1.5 MBq
2	400 μm	19 MeV	3.0 $\times$ 36 μAh	1.0 MBq
3	400 μm	19 MeV	3.0 $\times$ 176 μAh	2.0 MBq
4	400 μm	18 MeV	3.0 $\times$ 224 μAh	37.0 MBq

Tab. 2.5: Details of the ^{109}Cd production runs

400 mb maximum at 14 MeV should be considered as trustful for future runs. The resulting yield from this data is 0.06 $\frac{\text{MBq}}{\mu\text{Ah}}$.

The γ-spectrum of the source is shown in figure 2.9. Except for ^{109}Cd two other isotopes ^{106}Ag and ^{108}Ag respectively with 8.3 days and 418 years half-lives contribute in the γ-spectrum. Four produced sources are listed in table 2.5. During the irradiation of the first three sources the beam current was unstable. This is the reason why their activities are almost equal in quite of irradiation times. Activity of the fourth source matches the predicted yield well.

A use of a 100 % pure ^{109}Ag target can resolve the problem of the presence of ^{106}Ag and ^{108}Ag γ-lines. It will double the yield as well. Also this will contribute in better signal resolution: Firstly, contribution of 88 keV with 3.7 % intensity to the Compton background is small. Secondly, the intensities of 21.99 and 22.16 keV X-ray radiations sum up in 85.7 %.

To produce significant activity of ^{109}Ag for the space missions an application of cyclotrons with higher beam current and smaller beam diameter is recommended. Within the agreement between the University of Bonn and the TU Dresden a 0.37 GBq source of ^{109}Ag from Cyclotron Instruments [57] was purchased on 29.03.2010. The active diameter of the source of 1.2 mm is ideal for the XRD experiments.

To optimize the Signal-to-Noise-Ratio in XRD experiments trials with proportional chambers are in progress.

Conclusion

Feasibility of production of the ^{109}Cd at Bonn Cyclotron facility for the X-ray diffraction set-up projected in the TU Dresden was studied. For the interplanetary mission an irradiation at cyclotrons with higher particle current is of advantage: a cross section maximum of the reaction is pretty high. These cyclotrons have usually better focusing capabilities, which result in a point-source with an active diameter of order of millimeters. A usage of 100% pure ^{109}Cd target will double the production yield. This measure will also remove ^{106}Ag and ^{108}Ag γ-transitions presence from the spectrum. A 0.37 GBq source with a 1.2 mm active diameter from Cyclotron Instruments [57] was purchased. Studies to raise the Signal-to-Noise-Ratio are in progress. A use of a proportional chamber as a detector for XRD/XRF measurements is considered.

Chapter 3

Conclusions

It was shown that the production of ^{83}Rb from liquid, natural Br is feasible at the Bonn Cyclotron. A number of ^{83}Rb/^{83m}Kr generators were produced for test purposes of the University of Münster. The subsequent transformation of an irradiated target into a source, which can be attached to the KATRIN monitor spectrometer has been tested and is a comparably simple process. This is important considering the large amount of activity, which has to be handled in the planned experiments. Finally, it was found that ^{83m}Kr is released completely from the Rubidium Bromide (RbBr) residue retained in the quartz ampule after the evaporation of the excess Br. Surface effects in the capillary of the CKrS play a major role since the amount of emanated ^{83m}Kr atoms result in a disintegration in the order of 10^6 per second. Improvements of this procedure, like the use of isotopic enriched materials seem unnecessary at the moment since the possible gain of about a factor two compares unfavorably to the cost and availability of the necessary quantities of enriched Br. A possibility of ^{83}Rb implantation with 38 % efficiency is shown in the example of non-radioactive Rb implantation.

Alternative sources, ^{101}Rh and ^{109}Cd, for the extraterrestrial X-ray diffraction and X-ray fluorescence analysis applications were investigated. Their production by means of ^{99}Ru(d, 2n)^{101}Rh and ^{109}Ag(d, 2n)^{109}Cd nuclear reactions at the Bonn Cyclotron were optimized by means of studies based on SRIM simulation software so the maximum transmission of the characteristic X-rays 19.15 keV - 22.16 keV were achieved. A maximum activity 1.2 GBq of ^{101m}Rh and 35 MBq of ^{109}Cd were obtained.

The usage of ^{101m}Rh for the test trials and ^{101g}Rh for the XRD experiments found to be unappropriate: The γ-line of ^{101m}Rh 306.86 keV with an 81% emission

probability make a significant contribution to the Compton edge and background. It is expected that ^{101g}Rh source's γ-transitions at 127.23, 198.01 and 325.23 keV, with intensities varying from 11.8% up to 73% accompanying the X-ray emission will result in low Signal-to-Noise-Ratio.

The ^{109}Cd isotope implementation for the purposes of extraterrestrial XRD set-up was found to be suitable. For the interplanetary mission an irradiation at cyclotrons with higher particle current is recommended.

A few sources for trials of the XRD test set-up at the TU Dresden were produced. A 0.37 GBq source with a 1.2 mm active diameter from Cyclotron Instruments [57] was purchased. Raise of the Signal-to-Noise-Ratio by means of a proportional chamber detector application is under investigation.

Bibliography

[1] W. Pauli, *Rapports et discussions du septieme Conseil de physique sous les auspeces de l'Institut International de Physique Solvay* (Bruxelles, 1933) (Paris: Gautier -Villars 1934)

[2] J. S. Allen, Phys. Rev. **61**, 692 (1942)

[3] E. Fermi, Z. Physik. **88**, 161 (1934)

[4] F. Reines, C. L. Cowan, Nature **178**, 446 (1956); 523 (erratum);
C. L. Cowan *et al.,* Science **124**, 103 (1956)

[5] F. Reines, C. L. Cowan, Phys. Rev **113**, 273 (1959)

[6] G. Danby *et. al.,* Phys. Rev. Lett. **9**, 36 (1962)

[7] B. Pontecorvo, "Inverse β^--process" Chalk River Laboratory report PD-205, 1946

[8] R. Davis, Phys. Rev. **97**, 766 (1955)

[9] B. Cleveland *et. al.,* Astrophys. J. **496**, 505 (1998)

[10] J. Bahcall *et. al.,* Astophys. J. **555**, 990 (2001)

[11] M. Nakagawa *et. al.,* Prog. Theor. Phys. **30**, 727 (1963)

[12] B. Pontecorvo, Zh. Eksp. Teor. Fiz. **53**, 1717 (1967);
Sov. Phys. JETP **26**, 984 (1968)

[13] H. H. Chen, Phys. Rev. Lett. **55**, 1534 (1985)

[14] SNO Collaboration, Department of Physics, Stirling Hall,
Queen's University at Kingston, Kingston, K7L 3N6, Ontario, Canada

[15] B. Aharmim *et. al.,* Phys. Rev. C. **72**, 055502 (2005)

[16] R. G. H. Robertson and D. A. Knapp, Ann. Rev. Nucl. Part. Sci. **38**, 185 (1988)

[17] National Institute of Standards and Technology (NIST) http://www.physics.nist.gov/PhysRefData/Star/Text/contents.html/

[18] Japanese Evaluated Nuclear Data Library (JENDL) http://wwwndc.tokai.jaeri.go.jp/sae/actx/a/acl4077.txt/

[19] V. N. Levkovskij, Activation cross section nuclides of average masses (A=40-100) by protons and alpha-particles with average energies (E=10 - 50 MeV), Inter. Vesi. Moscow

[20] G. Beamson *et. al.,* J. Phys. **E13**, 64 (1980)

[21] A. Osipowicz *et. al.,* Los Alamos e-print archive hep-ex/0109033, September 21st, 2001

[22] A. Picard *et. al.,* Nucl. Instr. and Meth. **B63**, 345 (1992)

[23] V. M. Lobashev, P. E. Spivak, Nucl. Instr. and Meth. **A240**, 305 (1985), V. M. Lobashev *et. al.,* Nucl. Instr. and Meth. **A238**, 496 (1985)

[24] KATRIN Design Report 2004, FZKA 7090, 2005

[25] H. Kawakami *et al.,* Phys. Lett. **B256**, 105 (1991)

[26] R. G. H. Robertson *et al.,* Phys. Rev. Lett. **67**, 957 (1991)

[27] E. Holzschuh *et. al.,* Phys. Lett. **B287**, 381 (1992)

[28] W. Stoeffl, D. J. Decman, Phys. Rev. Lett. **75**, 3237 (1995)

[29] C. Kraus *et al.,* hep-ex/0412056

[30] V. M. Lobashev, Nucl. Phys. **A719**, 153c (2003)

[31] V. M. Lobashev *et al.,* Phys. Lett. **B460**, 227 (1999)

[32] C. Weinheimer *et al.,* Phys. Lett. **B460**, 219 (1999)

[33] D. Venos *et al.,* Appl. Rad. Isot. **63**, 323 (2005)

[34] R. B. Firestone, V. S. Shirley, Table of Isotopes, Version 1.0, March 1996

[35] NuDat2 Software of National Nuclear Data Center in Brookhaven National Laboratory, http://www.nndc.bnl.gov/nudat2/

[36] T. Thümmler *et al.,* New Jour. Phys. **11**, 103007 (2009)

[37] J. Kaspar, Diploma Thesis, Czech Technical University, Prague, 2003

[38] A. Hermanne *et al.,* Nucl. Inst. and Meth. **B187**, 3 (2002)

[39] M. Rasulbaev *et al.,* App. Rad. Isot. **66**, 1838 (2008)

[40] J. Kaspar *et al.,* Nucl. Inst. and Meth. **A527**, 423 (2004)

[41] SRIM simulation software, http://www.srim.org/

[42] Oxford Instruments, Tubney Woods, Abingdon, Oxfordshire, OX13 5QX, UK

[43] Amptek Inc., 14 De Angelo Drive, Bedford, MA 01730, USA

[44] T. Seyller *et al.,* Surf. Sci. **454**, 55 (2000)

[45] F. Sharipov, KATRIN internal report 10-ME-2102, 2003

[46] B. Ostrick, Ph.D. Thesis, University of Münster, 2009

[47] National Instruments Corporation, 11500 N Mopac Expwy, Austin, TX 78759-3504, USA

[48] Oak Ridge National Laboratory, 1 Bethel Valley Road, Oak Ridge, TN 37831, USA

[49] W. L. Bragg, Proc. Cambridge Phil. Soc. **17**, 43 (1913)

[50] Joint research centre, institute for advanced materials, Ispra establishment, I-21020 Ispra, Italy

[51] ZAG Zyklotron AG, Hermann-von-Helmholtz-Platz 1,
D-76344 Eggenstein-Leopoldshafen, Germany

[52] Astrium GmbH Claude-Dornier-Straße, D-88090 Immenstaad, Germany

[53] M. S. Uddin *et al.,* App. Rad. and Iso. **64**, 1013 (2006)

[54] P. P. Dmitriev *et al.,* Atom. Ener. **22**, 310 (1967)

[55] X. Peng *et al.,* Nucl. Inst. and Meth. **B68**, 145 (1992)

[56] UHU GmbH & Co. KG, Hermannstraße 7, D-77815 Bühl / Baden, Germany

[57] Cyclotron Instruments, Sattlerweg 11c, D-55128 Mainz, Germany

Acknowledgements

First and foremost I would like to thank my supervisor Privatdozent Dr. Reiner Vianden for granting me the opportunity to work under his supervision. I thank him for his patience, support and encouragement. It was a great pleasure to do Ph.D. studies in such a very nice working atmosphere.

I also would like to thank Prof. Dr. Karl Maier and Prof. Dr. Peter Herzog for finding time to explain me interesting physical effects. I want to thank Prof. Dr. Christian Weinheimer and Dr. Klaus Schlößer for having interesting discussions.

I am thankful to members of Promotion Comitee Privatdozent Dr. Akaki Rusetskiy and Prof. Dr. Sokolowky for being interested in my thesis.

I am very grateful for the support of my parents and brother, for their love, care and patience, and for sharing bright and difficult times in my life. Without them, this work would not be possible.

I would like to thank all my colleagues and friends for warm and sincere atmosphere in the group. Riccardo Valentini for helping me in all aspects of life and compiling my thesis. Jens Niederhausen for teaching me great examples of humanism. I bag everybody to excuse me, since I cannot resume the kindness they showed to me in this short acknowledgement page: Nicole Santen, Bettina Steitz, Katalin Biro, Krystyna Müller, Sandra Paulus, Sahar Hamidi, Theresa Negrini, Samanta Tagayeva, Aigasha Syddykova, Kim Yunnam, Dolgormaa Dashzeveg, Anna Arensz, Beatrix Boutton, Kim Jong-ah, Noh Yoengmi, Galina Weber, Adele, Thomas Geruschke, Ronan Nédélec, Valentin Germic, Jakob Penner, Patrick Keßler, Michael Steffens, Marius Arenz, Pavel Cojocaru, Christian Karrasch, Matthias Heinrichs, Ronnie Simon, Miroslav Žboril, Drahoslav Venos, Oleg Lebeda, Kim Wooyoung, Woo Saengtae, Shin Byongwook, Jing Songwook, Park Myongchul, Azamat Kutmanov, Hamid Yusupov, Asrar Inogomov, Ulughbek Sayfuddinov, Zafar Qambarov, Sherzod Kadyrov, Hurshid

Kadirov, Ernest Kulmirzayev and Dr. Shady Reyimkuliyev.

Special thanks to people who contributed with their hands in the current work, Fine Mechanics Shop, Electronics Lab, Secretary, Cyclotron, Isotope Separator's Personnel: Cornellia Noll, Margret Balci, Mechthild Paus, Andrea Kehr, Claudia Seifert, Barbara Mosblech, Detlef Wolf, Stefan Birkenbach, Berndt Kann, Oliver Rast, Achim Henny, Siegbert Lehmann, Dr. Konrad Peithmann, Siegfried Hinderlich and Albert Dahl.

Using this opportunity I would like to thank Madame Vianden for playing the role of a mother for the whole group. Prof. Dr. Ada Yul'yevna Leyderman I wish to thank for bringing the extraordinary world of theater in my life. I want to thank Nurgul Usubalieva for asking me everyday: *When will you finish your studies?*

Finally, on this occasion I want to express my gratitude to Bundesministerium für Bildung und Forschung for financial support of my studies, Dr. Dorris Thrun and Petra Weiß for their great work at Bonner International Graduate School, the Alien Office Bonn and the Embassy of the Federal Republic of Germany in Tashkent for their help.